

The Feasibility of Potentially Hazardous Asteroids Flybys Using Multiple Venus Gravity Assists

Vladislav Zubko

Space Research Institute (IKI) of the Russian Academy of Sciences, Profsoyuznaya st. 84/32, Moscow, 117997, , Russian Federation

Abstract

This work develops low-energy spacecraft (SC) trajectories using Venus gravity assists to study asteroids during heliocentric transfer segments between planetary encounters. The study focuses on potentially hazardous asteroids (PHAs) as primary exploration targets. This paper proposes a method for calculating SC trajectories that enable asteroid flybys after a Venus gravity assist. The method involves formulating and solving an optimization problem to design trajectories incorporating flybys of selected asteroids and Venus. Trajectories are calculated using two-body dynamics by solving the Lambert problem. A preliminary search for candidate asteroids uses an algorithm to narrow the search space of the optimization problem. This algorithm uses the V-infinity globe technique to connect planetary gravity assists with resonant orbits. The resonant orbit in this case serves as an initial approximation for the SC's trajectory between two successive planetary flybys. Four flight schemes were analyzed, including multiple flybys of Venus and asteroids, with the possibility of an SC returning to Earth. The proposed solutions reduce flight time between asteroid approaches, increase gravity assist frequency, and enhance mission design flexibility. The use of Venus gravity assists and resonant orbits ensures a close encounter with at least one asteroid during the SC's trajectory between two consecutive flybys of Venus, and demonstrates the feasibility of periodic Venus gravity assists and encounters with PHAs. The developed method was applied to construct trajectories that allow an SC to approach both co-orbital asteroids with Venus and PHAs via multiple Venus gravity assists. An additional study was carried out to identify asteroids accessible during the Earth-Venus segment in launch windows between 2029 and 2050.

Keywords: Asteroid exploration; Mission design; Gravity assists; Trajectory optimization

Introduction

The study of asteroids located in the inner region of the Solar System, with orbits interior to the Earth one, is crucial for understanding planetary evolution and assessing potential threats to Earth. Currently, astronomical catalogs contain over 1 million minor bodies, but only approximately 3,000 of them have been spectrally classified. This highlights the need for new methods to research and classify asteroids, utilizing both ground-based facilities and spacecraft (SC).

Spacecraft missions for asteroid exploration are gaining increasing relevance. These include flyby studies and sample collection operations with subsequent sample return from the 81P/Wild 2 comet and the (25143) Itokawa, (162173) Ryugu, and (101955) Bennu asteroids to Earth. To date, 20 missions targeting 39 small bodies have been completed¹. However, the active development of new concepts and projects in this area continues, accompanied by a growing number of publications and projects from various space agencies.

The exploration of Near-Earth Asteroids (NEAs) represents a particularly significant focus within asteroid research. In recent decades, landmark sample return missions including Hayabusa [1], Hayabusa-2 [2], and OSIRIS-REx (changed to OSIRIX-APEx) [3] have been successfully completed. More recently, the DART equipped with CubeSat LICIACube [4] asteroid redirection mission to the (65803) Didymos – Dymorphos system has demonstrated new capabilities for planetary defense, with follow-up missions such as Hera [5] coupled with two CubeSat Milani [6] and Juventas [7] currently in development. This growing interest in asteroid exploration has also enabled smaller, more focused missions like M-ARGO [8] and NEAScout [9, 10], highlighting the expanding diversity of approaches to studying these celestial bodies.

When designing trajectories for SC missions to asteroids, various strategies can be employed depending on a variety of factors. These factors include the number of target bodies, the use of gravity assists, and the type of propulsion system (chemical or electric). Typically, these trajectories are obtained by solving an optimization problem to find trajectories that meet criteria such as minimizing fuel consumption, minimizing flight time, or finding a balance when strict limits are imposed on any of these parameters.

The approaches can be broadly categorized as follows:

¹Based on an analysis of data from Jet Propulsion Laboratory (JPL) database <https://ssd.jpl.nasa.gov/sb/targets.html> (access date: 01.03.2025)

1. Approaches involving direct or multi-revolution transfer trajectories from Earth to asteroids without gravity assists [11, 12, 13, 9, 10, 14].
2. Approaches utilizing flight schemes that employ a combination of Earth and Venus gravity assists with subsequent entry into a heliocentric orbit with a significantly elongated aphelion. Such schemes often include a series of maneuvers near Venus and/or Earth. Examples of such trajectories are presented in works [15, 16, 17, 18, 19, 20]; a similar strategy was implemented in the Lucy mission [21].
3. Approaches utilizing the unstable dynamics of the few-body problem on various transfer segments, particularly — in the vicinity of the Sun-Earth system libration points. Aspects of the practical application of such dynamics are described in the works of [8, 22, 23, 24, 25, 26, 27].
4. Approaches using invariant manifolds in the vicinity of libration points in the Sun-Earth system for guidance and control of a station to be sent to study a comet/asteroid that passes near Earth [28, 29, 30, 31, 25].

It is important to note that the approaches described above can be applied to the design of either spacecraft trajectories or asteroid trajectories. The latter case is relevant for planetary defense or asteroid exploration concepts where the asteroid itself is the controlled body, as exemplified in [32, 33, 34].

The approaches in the first group, subject to stringent Δv constraints², primarily focus on trajectories that are suitable for exploring the near-Earth asteroids (NEAs) [12, 13, 11]. The second group focuses on Main Belt asteroids, which are the largest population of minor bodies. The approaches of this group focus on finding SC trajectories for encountering with Main Belt asteroids [35, 36, 37, 38, 19, 20]. The third group also targets near-Earth asteroids (NEAs), as it relies on gravitational effects from the n -body problem to achieve exhaust velocity enough to escape from Earth's sphere of influence (SOI) [22, 23, 24, 25, 26, 27].

Research from [15, 16] has demonstrated that high-thrust propulsion systems, combined with gravity assists from Venus, Earth, and in some cases Mars, enable targeting multiple objects during Earth-to-Earth transfers at sufficiently low cost. This approach requires only a single Δv maneuver³ for the initial flight to Venus, with negligible impulses required during subsequent gravity assist maneuvers. These studies showed that the patched-conic approximation significantly simplifies the initial search for candidate asteroids. A similar analysis was performed in [19], where the authors applied Bellman's optimality principle to identify trajectories for multiple encounters with Main Belt asteroids using an SC equipped with low-thrust engines.

Recent studies [39, 40, 41] have demonstrated the possibility of an asteroid encounter during the SC flight from Earth to Venus. In the article [39], ballistic schemes for Venus with possible launch periods between 2030 and 2040 were investigated. The analysis revealed that feasible trajectories for an asteroid encounter during the Earth-Venus transfer segment exist. In [40, 41], the authors analyzed a flight scheme in which, after a Venus gravity assist, the SC enters a resonant orbit⁴, allowing an asteroid flyby before the next encounter with the planet. The analysis used the patched-conic approximation and solved the Lambert problem for each trajectory, with flybys of one of 120 target objects. It showed that at least one flyby was possible within the proposed scheme. The launch dates for missions in previous studies were chosen to coincide with the planned Venusian missions between 2029-2035: *Venera-D* [42, 43, 44], *DAVINCI+* [45], *VERITAS* [46], and *EnVision* [47].

It should be noted that, despite similar ideas being presented in previous research [40, 41], where it was shown that an asteroid can be encountered by a spacecraft flying along a resonant 1:1 orbit, their scope was inherently limited to a single opportunistic flyby during a transfer trajectory designed for a specific planetary objective - landing on the surface of Venus. Therefore, those studies were more focused on reaching the desired region on Venus than on asteroid flybys.

This research focuses on the trajectories of the second group mentioned above. The main focus is on the trajectory for the SC using gravity assist maneuvers near Venus, which enables the SC to encounter asteroids while remaining near Venus's orbit, facilitating the simultaneous study of both the small bodies and the planet. This approach has the potential to significantly increase the effectiveness of multiple SC missions to asteroids and other planetary bodies for scientific purposes, thereby enhancing the scientific return of missions to the inner Solar System.

Four flight schemes were considered:

1. asteroid flyby without gravity assists with a return to Earth: Earth \rightarrow asteroid \rightarrow Earth;
2. asteroid flyby with gravity assists at Venus and without a return to Earth: Earth \rightarrow Venus \rightarrow asteroid \rightarrow Venus;
3. multiple asteroid flybys without return to Earth: Venus \rightarrow 1st asteroid \rightarrow Venus \rightarrow 2nd asteroid \rightarrow Venus \rightarrow p -th asteroid $\dots \rightarrow$ Venus;
4. multiple asteroid flybys with a return to Earth: Earth \rightarrow Venus \rightarrow asteroid \rightarrow Venus $\dots \rightarrow$ p -th asteroid \rightarrow Venus \rightarrow Earth.

Similarly to previously mentioned studies [18, 19, 35], this study uses the Lambert problem to determine the flight trajectories of SC between each pair of bodies. However, this research focuses primarily on asteroid exploration within

² Δv denotes a change in the characteristic velocity after the execution of a rocket-powered maneuver.

³ Δv denotes a change in the characteristic velocity resulting from a rocket-powered maneuver.

⁴Based on an analysis of data from the JPL database https://ssd.jpl.nasa.gov/tools/sbdb_query.html (access date: 01.03.2025)

a region close to the orbit of Venus, where the asteroid population is distinctive. For this reason, the research uses a methodology that includes a primary search for asteroid targets using the V-infinity globe approach, which connects gravity assist maneuvers with resonant orbits. This provides initial data for a subsequent search, using patched-conic techniques, for optimal flight trajectories.

Within this study, PHAs⁵ are considered as target objects for exploration. These objects are significant because of their potential threat to the Earth, making it particularly important to observe them from close distances.

An initial selection of asteroids from the Jet Propulsion Laboratory (JPL) database was performed. Subsequently, trajectories ensuring flybys with minimal Δv costs, including launch and interplanetary maneuver costs, were determined. Then, the Earth \rightarrow asteroid \rightarrow Earth schemes were compared with the scheme proposed in this work, which includes multiple Venus flybys.

The comparison showed that the multi-stage scheme does not significantly increase flight time and, in some cases, allows all flybys to be completed in a shorter time. The feasibility of returning the SC to Earth after a series of maneuvers was also demonstrated. For example, the SC trajectory using Earth \rightarrow Venus \rightarrow 1st asteroid \rightarrow Venus \rightarrow 2nd asteroid \rightarrow Venus \rightarrow Earth scheme was calculated. It was shown that such a return is possible in most cases of a transfer to an asteroid involving a Venus gravity assist.

The analysis revealed that using a 1:1 resonant orbit with the Venus orbit (having a period of ≈ 224.699 days) significantly reduces the transfer duration to asteroids. Calculations show that in some cases, a Venus gravity assist reduces the total impulse Δv compared to direct transfers when launch windows coincide. Moreover, transfers between Earth and Venus limit opportunities for flybys of asteroids, because the orientation of the SC orbits in this case depends on the position of both planets at the initial and terminal points, respectively. The use of resonant orbits allows aligning the SC's motion plane with the orbits of the target objects, thereby increasing the mission efficiency.

Another motivation for studying a particular region of space, namely the vicinity of the orbit of Venus, is the potential to discover unknown asteroids in an orbital resonance with Venus. A further significant objective is the investigation of the dust envelope located near the orbital distance of Venus [48]. Currently, only five such asteroids are known [39] and about 20 are suspected to be captured in resonance with the Venus orbital motion [49]. Therefore, the exploration of the SC orbits identified in the current paper could yield interesting results that can greatly contribute to the state of the art in this field. Therefore, the exploration of the SC orbits identified in the current paper could yield interesting results that can greatly contribute to the state of the art in this field.

Therefore, this work's novel contribution is twofold. First, it proposes, explores and validates the feasibility of Venus-asteroid-Venus flight schemes. Second, it presents techniques for calculating the initial parameters needed to optimize these trajectories in terms of total Δv . Additionally, the catalog of the optimal SC trajectories with asteroid flybys using multiple Venus gravity assists is provided for 2029 and 2031 launch windows.

The paper is structured as follows: the Introduction establishes the study's relevance and reviews different trajectory design approaches. The first section, Calculation Techniques (Section 1), is divided into subsections detailing the calculation of SC trajectories using the patched-conic approximation (Section 1.1), the construction of trajectories for multiple flybys (Section 1.2), and the specific technique for searching candidate asteroids (Section 1.3). The second section, Results (Section 2), presents the findings in subsections covering the selection of the target asteroid group (Section 2.1), a comparative analysis of different flyby schemes (Section 2.2), an example of a multi-asteroid flyby trajectory and an analysis of trajectories that return to Earth (Section 2.2.7), refining results in high-fidelity model (Section 2.3), a study of combined flight with Venus resonant asteroids and PHAs (Section 2.4), and a study of flybys on the Earth-Venus segment (Section 2.5). The summary of the advantages of the proposed methods as well as used flight schemes is provided in Conclusion (Section 4), followed by a section for Acknowledgments.

1. Methods

1.1. Interplanetary Flight Trajectory Design Using the Patched-Conic Approximation

For all considered flight schemes, the patched-conic method was used [50]. According to this method, the SC transfer trajectory between each pair of celestial bodies was considered as a conic section. The SOIs of these celestial bodies are contracted to a point in heliocentric motion. The SC transfer trajectory between two bodies was determined by solving the Lambert problem. This problem determines the heliocentric velocity vectors at the initial and terminal points of the motion based on known heliocentric position vectors for the initial and terminal positions, as well as the time of flight. In this work, Izzo's method was used to solve the Lambert problem [51].

Since the Izzo method allows calculating the transfer trajectory between two celestial bodies, even when the angular distance exceeds 2π , to avoid encountering with solutions involving multiple revolutions around the Sun, the maximum number was limited to four in this work.

The SC trajectory was calculated using the following algorithm:

1. The required number p of asteroid and k (with $k > p$) planetary encounters was defined.

⁵Potentially Hazardous Asteroids or PHAs are a special group of near-Earth asteroids for which the Minimum Orbit Intersection Distance (MOID) is less than 0.05 astronomical units, and the absolute magnitude is less than 22.

2. $s + 1$ transfer segments between each pair of celestial bodies were defined. The number of transfer segments is determined by $s = p + k$, and an additional segment is added corresponding to the Earth-Venus segment.
3. The SC position vectors at the initial time, planet flyby, and asteroid flyby at times t_j were defined as follows: $\mathbf{r}_0(t_0), \mathbf{r}_1(t_1), \dots, \mathbf{r}_j(t_j), \dots, \mathbf{r}_s(t_s), \mathbf{r}_{s+1}(t_{s+1})$.
4. The Lambert problems for each segment to obtain the velocities was solved and velocities at launch and each body encounter were obtained:

$$\mathbf{v}_0(t_0), \mathbf{v}_1(t_1), \dots, \mathbf{v}_j(t_j), \dots, \mathbf{v}_s(t_s), \mathbf{v}_{s+1}(t_{s+1}).$$

5. The asymptotic velocities at each planet flyby were calculated:

$$\mathbf{v}_{\infty,0} = \mathbf{v}_0 - \mathbf{v}_{pl,0}, \quad \mathbf{v}_{\infty,1} = \mathbf{v}_1 - \mathbf{v}_{pl,1}, \quad \dots, \quad \mathbf{v}_{\infty,j} = \mathbf{v}_j - \mathbf{v}_{pl,j} \dots, \quad \mathbf{v}_{\infty,s} = \mathbf{v}_s - \mathbf{v}_{pl,s}$$

6. The following cost function was defined:

$$\begin{aligned} G = \Delta v_{tot}(t_0, t_1, \dots, t_{s+1}) &= \Delta v_0(t_0, t_1) \\ &+ \sum_{j=1}^{s-1} [\Delta v_{\pi}(t_j, t_{j+1}) + \Delta v_{t_j}(t_j, t_{j+1}) + \Delta v_{ast}(t_{j+1}, t_{j+2})] \end{aligned} \quad (1)$$

where the components are defined as follows:

- $\Delta v_0 = \sqrt{2 \frac{\mu_E}{r_{LEO}} + (v_{\infty,0}^+)^2} - \sqrt{\frac{\mu_E}{r_{LEO}}}$ is the impulse required to launch from a low Earth orbit (LEO) with a radius of 6571 km; μ_E – gravitational parameter of the Earth.
- $\Delta v_{\pi,j} = \sqrt{2 \frac{\mu_{pl}}{r_{\pi,j}} + (v_{\infty,j}^-)^2} - \sqrt{2 \frac{\mu_{pl}}{r_{\pi,j}} + (v_{\infty,j}^+)^2}$ is the impulse at the planet's periapsis during its flyby, where $r_{\pi,j}$ is the periapsis radius; μ_{pl} – gravitational parameter of the planet.
- $\Delta v_{t,j}$ is the impulse required to adjust the velocity asymptote (in cases where the turn angle exceeds the natural one);
- $\Delta v_{ast,j} = \|\mathbf{v}_{ast,j}^- - \mathbf{v}_{ast,j}^+\|$ is the velocity change during asteroid flyby. The impulses described above were applied if the following condition for an unpowered (free) flyby was violated:

$$A_{min} \leq \arccos \frac{\mathbf{v}_{\infty,j}^- \cdot \mathbf{v}_{\infty,j}^+}{v_{\infty,j}^2} \leq A_{nat} \quad (2)$$

where $A_{min} = \arcsin(1/(1 + r_{SOI} v_{\infty,j}^2 / \mu_{pl}))$ and $A_{nat} = \arcsin(1/(1 + r_{\pi,min} v_{\infty,j}^2 / \mu_{pl}))$ are the minimum and natural turn angles of the asymptotic velocity, achieved at the distance of the planet's SOI (r_{SOI}) and minimum planet flyby distance ($r_{\pi,min}$) correspondingly.

7. The goal was to find the trajectory that minimizes:

$$G^* = \min_{t_0, t_1, t_2, t_3, t_4, \dots, t_{s+1}} \Delta v_{tot}.$$

A two-stage optimization algorithm was applied:

- A global search was performed to locate the region containing the global minimum of G^* . This search was performed using a meta-heuristic genetic algorithm from the evolutionary class of optimization techniques – differential evolution [52].
- A search for the exact minimum of the cost function G^* in the previously found region using a gradient-based Broyden-Fletcher-Goldfarb-Shanno algorithm [53].

8. After the optimization procedure, the following constraints are checked:

$$\begin{cases} \Delta v_0 \leq \Delta v_0^{lim} \\ \sum_{j=1}^{s-1} (\Delta v_{\pi,j} + \Delta v_{t,j}) \leq l_1 \\ \sum_{j=1}^{s-1} (\Delta v_{ast,j+1}) \leq l_2 \end{cases} \quad (3)$$

where Δv_0^{lim} is the limit on the launch impulse value, adopted according to technical constraints on existing upper stages of launchers; l_1 and l_2 are constraints on the total impulse for planetary flybys and asteroids, respectively.

In this work, Δv_0 value was set to 4.1 km/s, reflecting the current development of the rocket industry, which allows the use of liquid oxygen/hydrogen upper stages. The theoretical limit for this impulse is about 4.53 km/s, while the more realistic impulse is close to 3.49–3.62 km/s (for existing rockets)[54]. A value of $\Delta v_0^{lim} = 4.1$ km/s was chosen, consistent with current upper stage capabilities, although a detailed launch performance analysis was beyond the scope of this study.

Equation (3) imposes constraints on the total impulse for planetary flybys (the second constraint) and for asteroid flybys (the third constraint). The constraints on the total impulse for planetary and asteroid flybys depend on the number of asteroids in the flight scheme. For a scheme including one asteroid flyby, both constraints are set to 10^{-3} km/s, while for five or more asteroids, their values are taken as $l_1 = 0.1\Delta v_0^{lim}$ and $l_2 = 0.025\Delta v_0^{lim}$. The value $l_2 = l_1/5$, selected empirically, ensures that an asteroid flyby requires a significantly lower impulse than a planetary flyby.

It can be noticed that for trajectories satisfying the condition $\sum_{j=1}^2 (\Delta v_{\pi,j} + \Delta v_{t,j} + \Delta v_{ast,j+1}) \leq 10^{-3}$ km/s, the duration between successive planetary gravity assists fall into one of two categories:

$$\begin{aligned}\Delta t_{j,j+2} &= \sum_{j=1}^2 (t_{j+1} - t_j) \neq nP_{pl}, \\ \Delta t_{j,j+2} &= \sum_{j=1}^2 (t_{j+1} - t_j) \approx nP_{pl}.\end{aligned}\quad (4)$$

where P_{pl} is the planet's orbital period.

The above relations imply that for a transfer trajectory obtained by connecting transfer segments initiating and terminating on the same celestial body, the heliocentric trajectory of the SC can be approximated by corresponding $m : n$ resonant orbits connecting at the moment of the asteroid approach. Based on this, one can formulate the simplification to the cost function.

Simplification 1. The cost function (1) is modified assuming that the SC transfer duration between two successive Venus flybys is known and exactly equals nP_{pl} days, then $t_{j+2} = nP_{pl} + t_j$. Thus, the original cost function (1) can be rewritten as

$$\tilde{G} = \Delta v_0(t_0, t_1) + \sum_{j=1}^{s-1} [\Delta v_{\pi}(t_j, t_{j+1}) + \Delta v_t(t_j, t_{j+1}) + \Delta v_{ast}(t_{j+1}, t_j + nP_{pl})] \quad (5)$$

The obtained cost function is then minimized $\tilde{G} \rightarrow \min$ over the set of time moments t_0, t_1, \dots, t_s .

These rules for transfer segment sequence and duration (indexed by j) apply to SC trajectories that include an Earth-to-Venus segment. Alternatively, when such a segment is absent, for example, in an Earth-asteroid-Earth flight scheme, the number of segments are reduced by one and the algorithm described in this section can be applied similarly.

1.2. Construction of Trajectories for Planetary and Several Asteroid Flybys

The method established in Section 1.1 is suitable for determining an optimal trajectory for a predefined sequence of bodies. It allows us to easily solve the problem of determining the optimal trajectory when the SC passes only one asteroid. However, when the number of encountered asteroids exceeds one, it becomes necessary to conduct a preliminary search for suitable candidate asteroids and determine the range of possible flyby dates.

This section provides an algorithm for the preliminary selection of candidate asteroids at each flyby of the planet. The geometric relationship is used to approximate the SC trajectory with a resonant orbit. A V-infinity globe approach, which connects gravity assists and resonant orbit design in a two-body problem, is used to determine the initial turn angle. This initial angle is determined by the requirement for close encounters between the SC and an asteroid on a resonant orbit.

Assuming, to a first approximation, that the eccentricity of Venus's orbit is negligible, a set of unit vectors describing a coordinate system suitable for asymptotic velocity transformations are written as:

$$\xi^0 = \frac{\mathbf{v}_{pl}}{\|\mathbf{v}_{pl}\|}, \quad \zeta^0 = \frac{\mathbf{r}_{pl} \times \mathbf{v}_{pl}}{\|\mathbf{r}_{pl} \times \mathbf{v}_{pl}\|}, \quad \eta^0 = \xi^0 \times \zeta^0 \quad (6)$$

where ζ^0 points along the planet velocity vector, ζ^0 is directed along the angular momentum vector, and η^0 completes the dextral orthonormal triad.

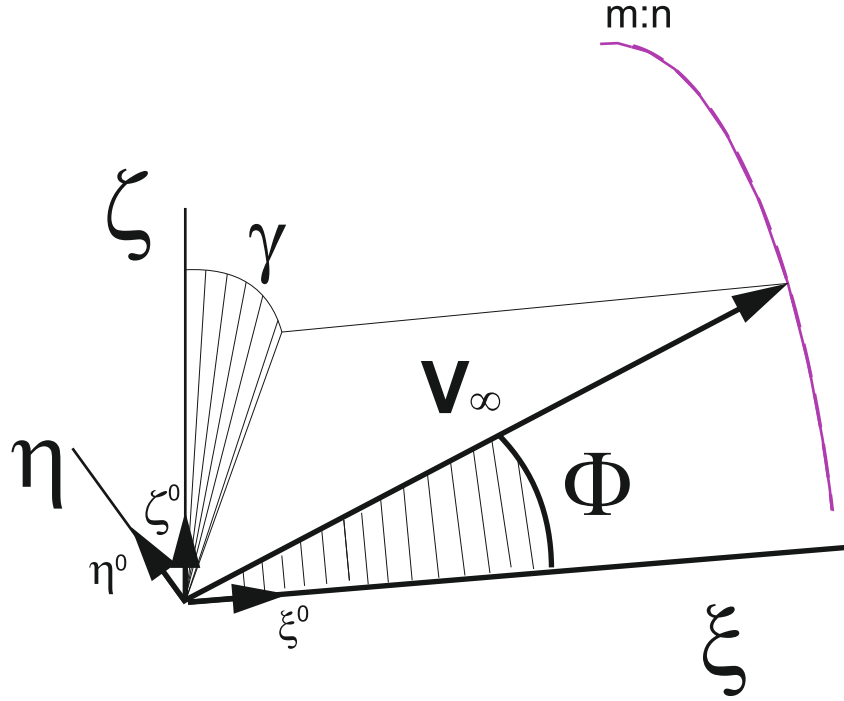


Figure 1: SC asymptotic velocity at Venus flyby in the $\xi\zeta\eta$ coordinate system

The asymptotic velocity vector of the SC at the Venus flyby is shown in Figure 1. In the coordinate system (6), the vector \mathbf{v}_∞ can be defined by introducing angles Φ, γ ⁶ as follows:

$$\mathbf{v}_\infty = v_\infty [\cos \Phi, \sin \Phi \sin \gamma, \sin \Phi \cos \gamma]^T. \quad (7)$$

Therefore, the SC state vector (heliocentric position vector of SC \mathbf{r}_{pl} , and heliocentric velocity vector \mathbf{v}_{pl}) after Venus gravity assist can be written as:

$$[\mathbf{r}_{sc}, \mathbf{v}_{sc}] = [\mathbf{v}_{pl}, \mathbf{v}_{pl} + \Xi \mathbf{v}_\infty]. \quad (8)$$

where Ξ is the state transition matrix from $\xi\zeta\eta$ to Heliocentric ecliptic J2000 coordinate system.

Assuming that $\mathbf{v}_\infty = \text{const}$ during the Venus flyby, the m:n resonant orbit is completely determined by Φ, γ , where Φ completely determines the $m : n$ ratio, and γ determines the orientation of the resonant orbit relative to the planet's orbital plane at $\Phi = \text{const}$. Thus, further in the work, by fixing the value of Φ , the resonant orbit is defined by the parameter γ .

Note that the theoretical investigation of resonant orbit design was conducted in [57, 56] while the general case of resonant and non-resonant double planetary flybys was widely described and analyzed in the paper [58].

1.3. Algorithm for Rapid Search for the Candidate Asteroids

Resonant orbits serve as an initial guess for constructing the SC trajectory, allowing an asteroid flyby (defined as $\Delta v \leq 1 \text{ m/s}$). Therefore, to select candidates from the entire set of asteroids, the following algorithm is used:

The core idea of the proposed approach is illustrated in Fig. 2. The figure depicts the set of resonant orbits formed by possible resonances available at the current v_∞ value during the Venus approach. An asteroid whose orbit intersects this set of orbits can have a close encounter with one of the resonant trajectories. Therefore, if such an encounter occurs at a sufficiently small distance—small enough to be compensated during the full optimization process described in Section 1.1—then the asteroid is included in the set of candidate asteroids.

⁶The angles Φ, γ introduced in this work follow [40, 55]), while in other papers these angles may be denoted differently, usually they are called Öpic variables [56] and denoted θ, ψ ; in [57] the notations α, κ are used; in [58] the notations ξ_1, ξ_2 are used.

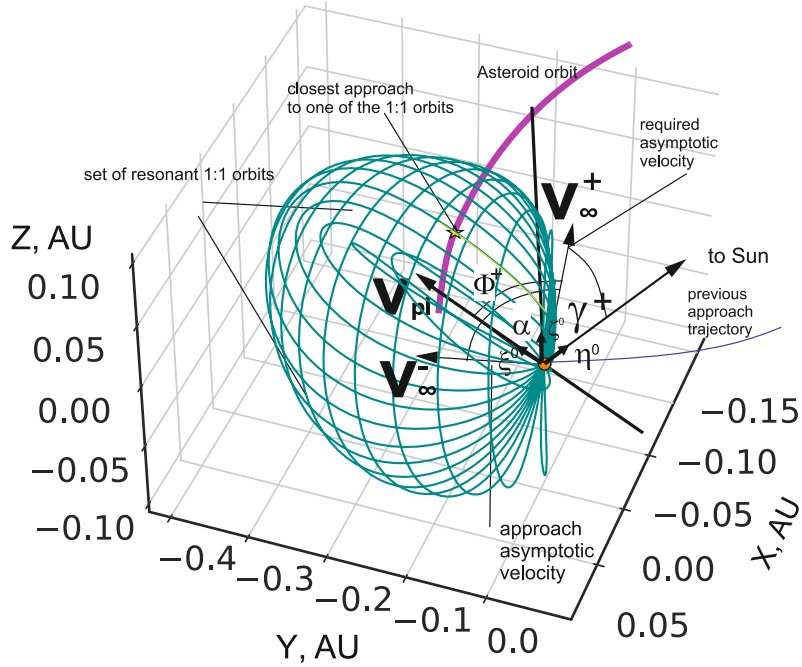


Figure 2: The geometric interpretation of the proposed technique

The algorithm for finding suitable candidate asteroids, based on the core idea presented and illustrated above, is provided in 1.

Algorithm 1: Selection of candidate asteroids and construction of trajectories for multiple asteroids flybys

Input: Set of PHAs \mathcal{A} , time of SC and Venus encounter t_j ; position and velocity of SC in heliocentric coordinates $\mathbf{r}(t_j), \mathbf{v}(t_j)$; maximum allowed MOID value: ρ_{max} ; maximum allowed value of minimum distance between SC and an asteroid on interval (t_j, t_{j+2}) , where $t_{j+2} = t_j + n P_{pl}$; $\Delta r_{\min}^{\text{lim}}$ maximum allowable minimum approach distance between SC and an asteroid; A_{nat} ; $\Phi(m : n, v_{\infty, j}) = \text{const}$

Output: Set of candidate asteroids \mathcal{A}_c

foreach asteroid $a \in \mathcal{A}$ **do**

Compute the minimum MOID between the SC's orbit and the asteroid's orbit over γ : $(\rho_{\text{moid}}^{\text{sc-ast}})_{\min} = \min_{\gamma} \rho_{\text{moid}}^{\text{sc-ast}}(\gamma)$;

$\tilde{\theta}_{j+1} = f(\theta_j, (\rho_{\text{moid}}^{\text{sc-ast}})_{\min})$ is the true anomaly of the SC at the minimal intersection point between the SC and asteroid orbits ;

$\tilde{t}_{j+1} = f(\tilde{\theta}_{j+1})$ is the time in UTC at which the SC reaches the specified position θ_j ;

$\tilde{\gamma}^+ = \arg \min_{\gamma} \rho_{\text{moid}}^{\text{sc-ast}}(\gamma)$ is parameter at which the minimum value of the MOID parameter is achieved among all resonant orbits of a given $m : n$;

if $\rho_{\text{moid}}^{\text{sc-ast}} \leq \rho_{\text{moid}}^{\text{max}}$ **then**

Determine $\Delta r_{\min}^{\text{sc-ast}} = \min_{\substack{\tilde{\gamma}^+ - \gamma^{\text{lim}} \leq \gamma \leq \tilde{\gamma}^+ + \gamma^{\text{lim}} \\ \tilde{t}_{j+1} - \delta t^{\text{lim}} \leq t \leq t_{\text{enc}} + \delta t^{\text{lim}}} \|\mathbf{r}(t, \gamma) - \mathbf{r}_{\text{ast}}(t, \gamma)\|$;

if $\Delta r_{\min}^{\text{sc-ast}} < \Delta r_{\min}^{\text{lim}}$ **then**

Check the condition: $A_{\min} \leq \arccos(\tilde{\mathbf{v}}_{\infty} \cdot \tilde{\mathbf{v}}_{\infty}^+) \leq A_{\text{nat}}$;

where $\tilde{\mathbf{v}}_{\infty} = \frac{\mathbf{v}_{\infty}}{v_{\infty}}$;

if constraint is satisfied **then**

Add a to \mathcal{A}_c ;

Determine $[t_{j+1}^*, \gamma^{**}] = \arg \min_{\substack{\tilde{\gamma}^+ - \gamma^{\text{lim}} \leq \gamma \leq \tilde{\gamma}^+ + \gamma^{\text{lim}} \\ \tilde{t}_{j+1} - \delta t^{\text{lim}} \leq t \leq t_{\text{enc}} + \delta t^{\text{lim}}} \|\mathbf{r}(t, \gamma) - \mathbf{r}_{\text{ast}}(t, \gamma)\|$;

return \mathcal{A}_c ;

It should be noted that the threshold values for the algorithm when used in this work framework were selected empirically through multiple simulations. The motivation for choosing empirical values stems from the highly nonlinear dependence of between Δr , ρ_{moid} and v_{∞} , γ , even at a fixed Φ value. In the considered case, the true anomaly at which the closest encounter occurs is a critical parameter for selecting appropriate threshold values for Δr and ρ_{moid} . However, this specific problem was beyond the scope of the current research, and the final threshold values were chosen to ensure a comprehensive initial search. The objective of this paper was to first identify suitable asteroids, then subject this set to the optimization problem, and finally filter them to obtain optimal trajectories. Therefore, the purpose of this algorithm is to narrow the search space for optimal trajectories that would ensure nearly impulse-free flybys of asteroids and, preferably, planets.

The following empirical values were used for the limiting parameters: $\Delta r_{\min}^{\text{lim}} = 5$ million km, $\rho_{\text{moid}}^{\text{max}} = 5$ million km, $\gamma^{\text{lim}} = 15^\circ$, and $\delta t^{\text{lim}} = 15$ days. The parameter $\rho_{\text{moid}}^{\text{sc-ast}}$ (also designated as ρ_{moid}) represents the minimum distance between the orbits of the SC and the asteroid and was calculated using an analytical algorithm from [59]. After compiling the candidate set, the steps from Section 1.1 were repeated for each asteroid in \mathcal{A}_c , with the optimization problem size increased by two additional segments.

Remark. This work uses an analytical approximation of the MOID parameter (designated as AMOID in [59]), which allows for approximating the characteristic change in the minimum distance between the orbits of the SC and the asteroid near local minima. However, since this approximated parameter (AMOID) can differ significantly from the true MOID, the search algorithm accounts for this potential error by using an initially overestimated value for $\rho_{\text{moid}}^{\text{sc-ast}} \leq \rho^{\max}$. Furthermore, the value of $\rho_{\text{moid}}^{\text{sc-ast}} \leq \rho^{\max}$ is chosen considering that the minimum MOID and $\Delta r_{\text{min}}^{\text{sc-ast}}$ may occur at different values of γ .

For example, Fig. 3 shows three different curves: AMOID, MOID, and $\Delta r_{\text{min}}^{\text{sc-ast}}$ plotted against γ for the 2000 DO1 asteroid. Figure 3 shows that the AMOID curve generally approximates the MOID values near the minimum, while the extremum of $\Delta r_{\text{min}}^{\text{sc-ast}}$ is different (shifted several degrees to the right in γ)

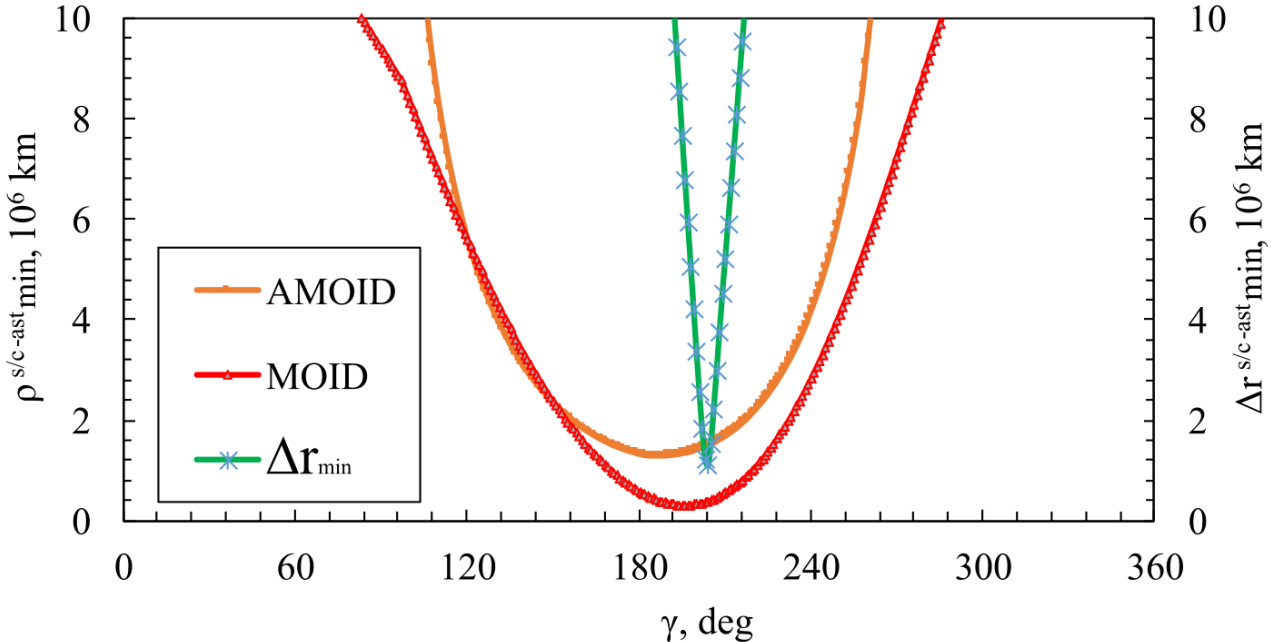


Figure 3: Comparison of the AMOID, MOID curves and the minimum distance between the SC and the asteroid as a function of the 1:1 resonant orbit, as a function of the parameter γ .

2. Results

2.1. Selection of Target Group of Asteroids From International Catalogs

To identify suitable asteroid targets for the proposed Venus flyby missions, a comprehensive search using the NASA Jet Propulsion Laboratory (JPL) Navigation and Ancillary Information Facility (NAIF) database was conducted, which contains orbital data for over 1.5 million small Solar System bodies. The selection process employed the following sequential filtering criteria:

- **Initial PHA Selection.** From the total database of 1,467,232 asteroids, at first about 2,500 objects are classified as Potentially Hazardous Asteroids (PHAs) according to JPL and Minor Planet Center databases.
- **Earth MOID Restriction.** To focus on objects with the highest Earth-impact risk, asteroids with Minimum Orbit Intersection Distance $\rho_{\text{moid}} \leq 1.05\text{LD}$ (where $1\text{LD} = 384,000$ km) were selected. This criterion identified 139 candidate asteroids that formed the primary target set for initial mission design.
- **Orbit Determination Precision.** To ensure reliable trajectory design, the strict uncertainty thresholds to orbital elements were applied:
 - Semi-major axis: $1-\sigma(a) \leq 10^{-5}$ au
 - Perihelion distance: $1-\sigma(q) \leq 10^{-5}$ au
 - Eccentricity: $1-\sigma(e) \leq 10^{-5}$
 - Angular elements (inclination, longitude of ascending node, argument of perihelion, mean anomaly): Total angular uncertainty $\leq 10^{-4}$ rad

Application of these uncertainty filters to the complete PHA dataset resulted in 2,030 well-characterized objects. The intersection of this refined set with the MOID-based selection yielded to the final target group of 139 asteroids. Figure 5 illustrates the distribution of orbital parameter uncertainties across the selected asteroids.

The target group includes both numbered and unnumbered asteroids to ensure comprehensive mission planning. While unnumbered asteroids currently present greater orbital uncertainty, they represent valuable future targets as orbit determinations improve. Figure 4 shows the distribution of orbital parameters for the final selection of 139 asteroids.

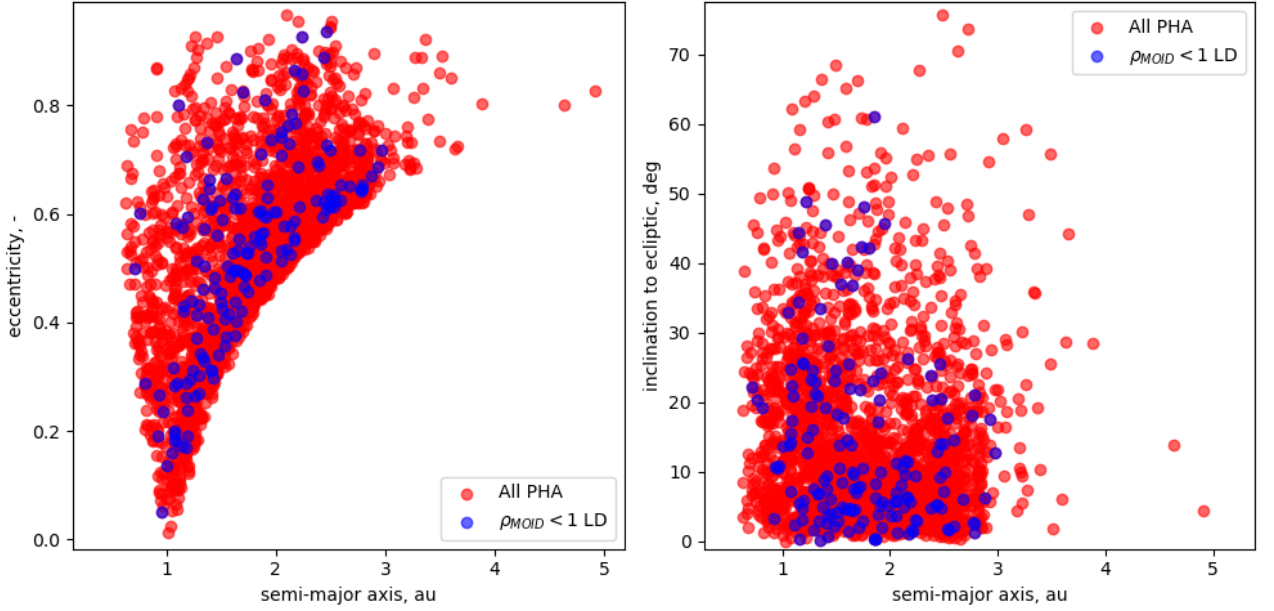


Figure 4: Distribution of orbital parameters for selected asteroids, showing semi-major axis versus eccentricity of their heliocentric orbits.

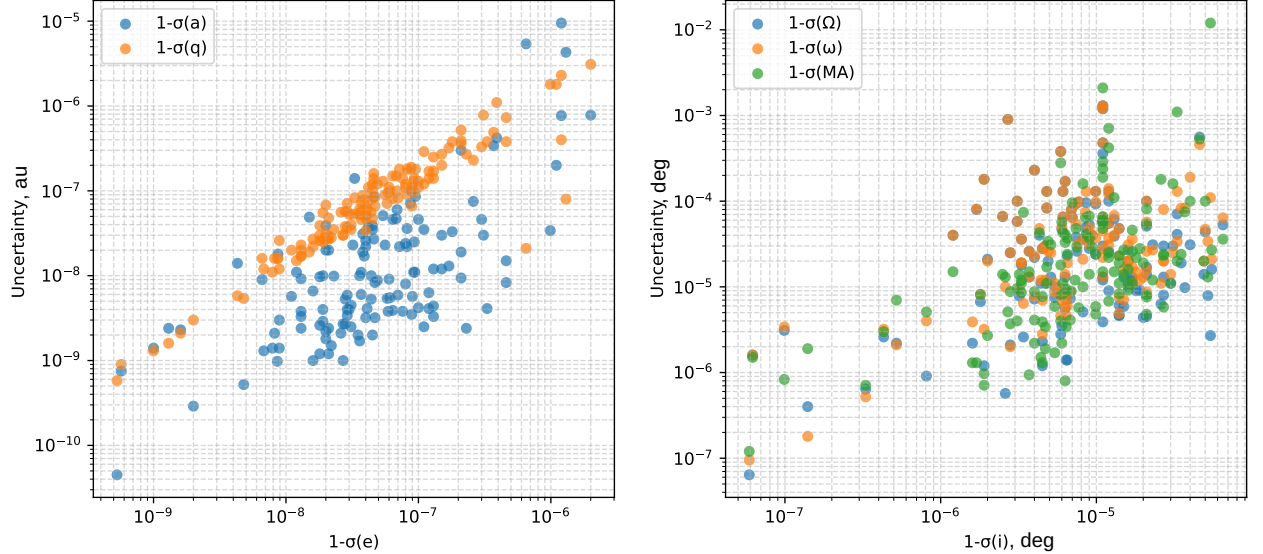


Figure 5: Distribution of uncertainties in orbital parameters for the selected asteroid group.

Although asteroids satisfying $\rho_{\text{MOID}} \leq 1.05\text{LD}$ have orbits that bring them near Earth's orbital path, the actual collision risk remains low. Only a small subset of these 139 objects are projected to approach within one lunar distance in the foreseeable future. Table 1 provides representative examples of close-approach parameters for selected asteroids, including minimum approach distances to both Earth and the Moon, where available⁷.

In Table 1, d_{\min} is the minimum approach distance of the asteroid to Earth on the given date.

As shown in Table 1, only a small fraction of the selected 139 objects approach Earth closer than 1 LD and thus pose little danger in the coming century. Nevertheless, constant refinement of the physical characteristics and orbits of these objects is a critical parameter in assessing their danger to the planet in the future.

In cases where flybys of several asteroids are studied, an extended catalog of objects is used. This includes all known PHAs as of July 2025 that satisfy the constraints above - 2030 objects.

⁷<https://naif.jpl.nasa.gov/naif/> (Access date 25.07.2025)

Table 1: Asteroids with $\rho_{MOID} \leq 1.05LD$ and $d_{min} < 10 LD$

Name	Celestial Body	Date and time of approach (UTC)	d_{min} (LD)	ρ_{MOID} (LD)
(35396) 1997 XF11	Earth	26.10.2028 06:44	2.417	0.158
1997 XF11	the Moon	26.10.2028 07:39	3.451	-
(279744) 1998 KM3	Earth	27.10.2095 01:03	5.099	0.983
(308635) 2005 YU55	the Moon	07.11.2075 23:50	0.601	-
2005 YU55	Earth	08.11.2075 07:24	0.53	0.182
2009 XT6	Earth	17.12.2112 01:15	7.229	0.866
(835579) 2011 SM68	Earth	17.10.2072 15:25	1.877	0.267
2011 SM68	the Moon	17.10.2072 17:36	1.713	-
2016 FG60	Earth	22.07.2112 17:59	8.253	0.124

2.2. Trajectories of Potentially Hazardous Asteroids Flybys

This section compares two schemes for asteroid flybys:

1. E-V-A-V = Earth-Venus-Asteroid-Venus,
2. E-A-E = Earth-Asteroid-Earth.

To simplify the scheme descriptions, the following designations are used: 'P' for a planetary flyby (Venus), and 'A' for an asteroid flyby.

For the study, 139 asteroids were selected (see Section 2.1). Trajectories were constructed for each of these asteroids according to the schemes described in Introduction Section, using the methods outlined in Sections 1.2 and 1.3. Trajectories that did not satisfy the constraints in Eq. (3) were excluded from further analysis. Two possible launch periods were considered: 2029 and 2031. The rationale for concentrating on these years is that many missions were planned to be launched to Venus, as described in the introduction.

In this section, comparisons are made between the times of flight from a low Earth orbit to encounter with Venus after asteroid flybys. Also, comparisons of Δv_0 values and asymptotic velocities at planetary and asteroid flybys are presented.

2.2.1. General Analysis of Results

Fig. 6 shows the total transfer duration for each of the considered schemes as a function of the launch date. The diagram shows results only for those asteroids (out of 139) for which a flyby was possible under the restrictions of Eq. (3). Table 2 shows the number of optimal flight trajectories that satisfy the constraint in Eq. (3). These were found for launch periods where asteroid flybys are possible under the studied schemes. Most complete data characterizing flight trajectories found during the study period for launch dates are provided in Tables A.1 and A.2 in Appendix A.

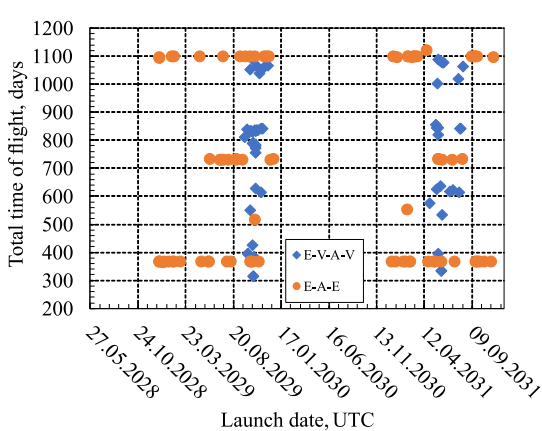


Figure 6: Total transfer duration for the two studied schemes vs the launch date

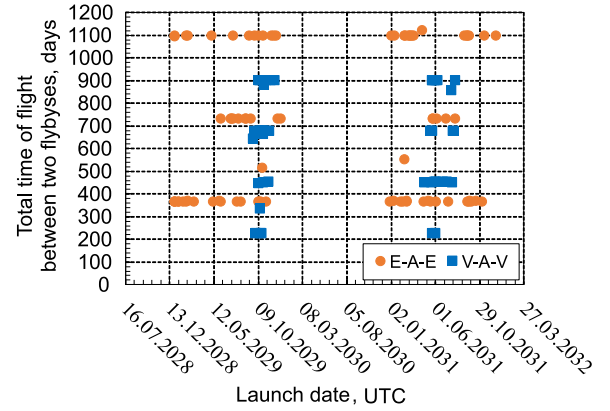


Figure 7: Transfer duration between two successive planetary flybys for the two studied schemes versus the launch date

Figure 6 shows the distribution of flight times from the initial point to the terminal point, including flybys of specific asteroids from the selected set. Analysis of this figure shows that the duration of the first trajectory (E-V-A-V) is generally shorter than the second (E-A-E). This is due to the shorter orbital period of Venus, which reduces the time between successive planetary encounters, thereby increasing the frequency of gravity assists. This provides a basis for finding subsequent candidate asteroids that can be encountered after the next Venus flyby.

It is possible to classify all calculated trajectories according to $m : n$ resonance on the P-A-P segment, based on the calculated flight time between two successive planetary encounters. The total flight duration presented in Fig. 6, allows such analysis only for the E-A-E scheme. For the E-V-A-V scheme, the duration of the V-A-V segment can be calculated

by subtracting the E-V duration from the total time of flight (see Fig. 7). Therefore, for each optimal trajectory using the method from Section 1.1, the classification has been outlined in Table 2.

Table 2: Distribution of trajectories on the P-A-P transfer segment by resonant ratios $m : n$

$m : n$ / launch year	V-A-V		E-A-E	
	2029	2031	2029	2031
1 : 1	4	2	28	21
3 : 2	21	5	-	-
2 : 1	8	14	13	15
no resonance	2	-	1	2
total	56	80		

Most of the transfer trajectories found involved asteroid flybys in $m : n$ resonant orbits, as seen from Fig. 6 and Table 2. The V-A-V flight trajectory corresponding to a 3 : 2 resonant orbit was the most frequently occurring for launches in 2029. The most frequently encountered resonant ratio allowing a flyby of an asteroid when launched directly from Earth was 1 : 1 for launches in both 2029 and 2031.

In the case of the E-A-E scheme, the frequent occurrence of 1 : 1 resonant orbits as a result of patching together the E-A and A-E trajectory parts can be easily explained by the initial small MOID between Earth's orbit and the asteroid's. Therefore, orbits with semi-major axes close to that of Earth are chosen. For the E-V-A-V scenario, the semi-major axes should be chosen such that they intersect with the Venus orbit. Since the initial MOIDs for orbits of Venus and the asteroids vary, the $m : n$ ratio varies more in this case.

2.2.2. Comparison of E-A-E and E-V-A-V Schemes

This section compares the E-A-E and E-V-A-V flight schemes, using parameters Δv_0 and v_∞ , for asteroid flybys, vs. the launch date. A separate analysis of v_∞ , at Venus, for the corresponding scheme, was also performed for the E-V-A-V scheme.

To perform a detailed analysis of the E-V-A-V scheme, a comparison was made between this scheme and the Earth-Venus (E-V) transfer. Typically, solutions to the Lambert problem for the E-V scheme are divided into two trajectory families. The first family includes trajectories for which the angular distance of flight is less than π ; the second family includes those where this distance is greater than π . These trajectory families facilitate the analysis of the initially studied E-V-A-V scheme.

In total, using the method described in Section 1.1, optimal trajectories were found for flybys of 56 asteroids using the E-V-A-V scheme and for 80 asteroids using the E-A-E scheme, for two launch windows in 2029 and 2031.

Fig. 8(a) compares the required ΔV_0 for transfer to asteroids using the E-A-E and E-V-A-V schemes. The Δv_0 requirements for single-revolution E-V transfers (for both solution families) are also shown in Fig. 8(a).

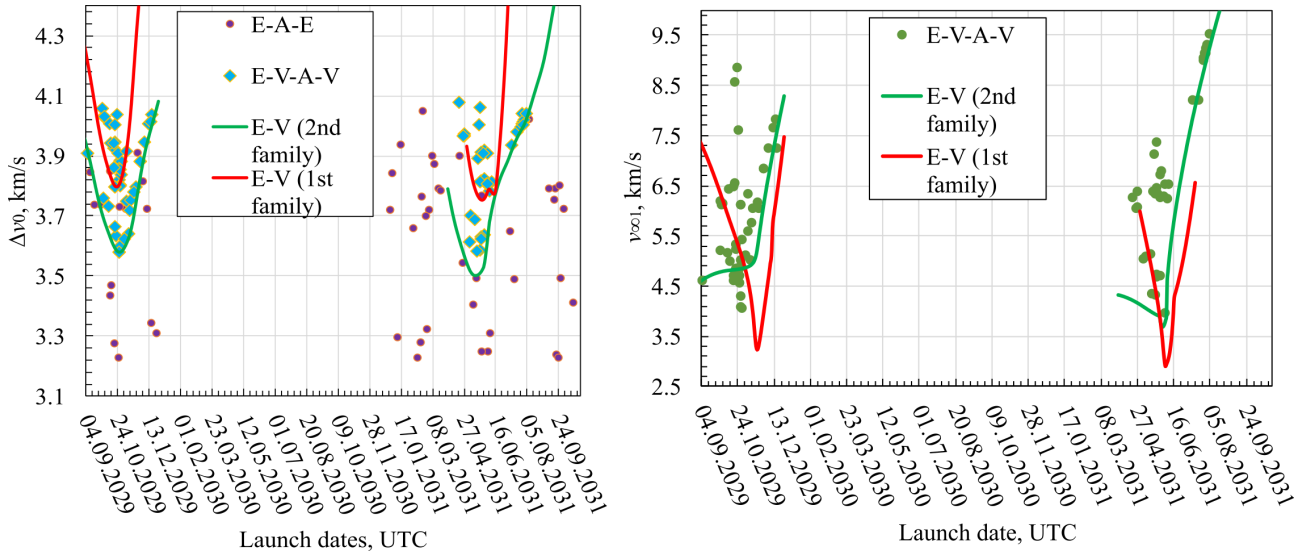


Figure 8: (a) Dependence of Δv_0 on launch date for the E-A-E and E-V-A-V schemes; (b) Dependence of $v_\infty,1$ for Venus flyby in the E-V-A-V scenario

Figure 8(a) shows that the E-A-E scheme typically requires lower Δv_0 than the E-V-A-V scheme. This is expected since the Δv_0 for Venus-assisted transfers cannot be lower than that of optimal single-revolution Earth-Venus transfers, which provide the theoretical minimum. The observed minimum Δv_0 for E-V-A-V trajectories is approximately 3.6 km/s, closely matching the optimal direct Earth-Venus transfer requirement.

Analysis of the Δv_0 distribution reveals that E-V-A-V values cluster near the minima of single Earth-Venus transfers. Most E-V-A-V Δv_0 values fall between the first and second solution family curves of direct transfers, with approximately half exceeding the second family's optimal values. This indicates that in these cases, faster transfers to Venus are required to enable subsequent asteroid encounters compared to optimal direct Earth-Venus trajectories.

The asymptotic velocities v_∞ at Venus approach (Fig. 8(b)) for E-V-A-V trajectories align closely with optimal direct Earth-Venus transfers. However, the requirement for impulse-free asteroid flybys generally results in v_∞ values exceeding both transfer families' optima. The few cases with lower v_∞ correspond to trajectories requiring higher Δv_0 for faster Venus transfers, as noted in the Δv_0 analysis.

Asteroid flyby velocities v_{ast} (equivalent to $v_{\infty,2}$ in E-V-A-V schemes) range from 2.3 to 44 km/s for both mission architectures (Fig. 9). The minimum v_{ast} values for E-V-A-V trajectories occurred during flybys of asteroids 2005 YU55 (2.3 km/s) and 2011 DV (6.975 km/s), with spacecraft motion on the Venus-Venus segments following 2 : 1 and 1 : 1 resonant orbits, respectively.

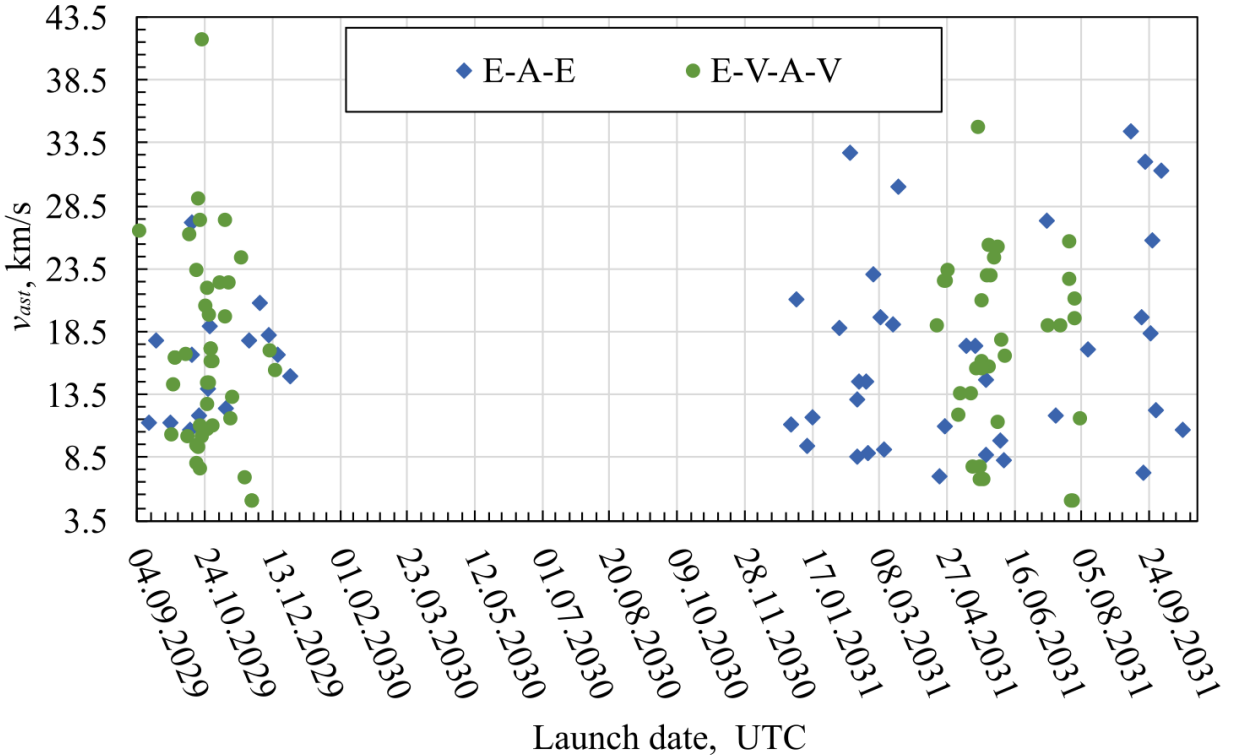


Figure 9: Dependence of v_{ast} on launch date within the launch windows in 2029 and 2031.

To summarize this section:

1. It was demonstrated that flybys of PHAs are feasible while the spacecraft moves along resonant orbits with Venus. This approach does not increase the total flight time and actually reduces the duration between successive planetary encounters compared to direct Earth-asteroid transfers.
2. Analysis of Δv_0 for both schemes revealed that while E-A-E transfers generally require lower launch impulses for this specific asteroid subgroup, the E-V-A-V scheme provides critical advantages in mission flexibility. Specifically, it enables shifted launch windows and creates additional launch opportunities to reach target asteroids while maintaining the capability for spacecraft return and subsequent maneuvers.
3. The E-V-A-V scheme demonstrates close alignment with optimal direct Earth-Venus transfers in terms of total Δv consumption (approximately equal to Δv_0 in the considered cases) and asymptotic velocity v_∞ at Venus flybys, validating its efficiency within the Venus gravity assist based mission architecture.
4. It was demonstrated that Simplification 1 (introduced in Section 1.1) can effectively reduce the optimization parameter space for missions involving asteroid flybys with return to the same planetary body. This simplification is justified by the observation that optimal asteroid encounters typically occur outside the planet's orbital plane, with the complete trajectory between planetary encounters connected through resonant orbits at the asteroid flyby points.

2.2.3. Construction of Multiple-Asteroid Flyby Trajectories Using Venus Gravity Assists

This section extends the Earth-Venus-Asteroid-Venus (E-V-A-V) scheme to include multiple asteroid flybys, where each additional asteroid introduces two additional V-A-V segments. The methodology employs geometric relationships within a two-body dynamics framework (see Sec. 1.3), focusing on the 2029-2031 launch windows.

The initial conditions for constructing multi-asteroid trajectories are derived from the single-asteroid flyby cases analyzed in the previous section, which are summarized in Table 3.

Among all considered trajectories, those enabling nearly impulse-free asteroid flybys while operating on 1:1 resonant orbits are particularly advantageous (Table 3). These solutions combine minimal energy requirements with the capability for repeated encounters over relatively short time intervals, making them ideal candidates for extended mission sequences.

Table 3: Schemes for flybys of asteroids on a 1:1 resonant orbit

Name	Launch Date (DD.MM.YYYY)	Duration, days			$v_{\infty,0}$, km/s	$v_{\infty,1}$, km/s	$v_{\infty,2}$, km/s	$\tilde{H}_{\pi}, 10^4$ km
		T_1 , days	T_2 , days	T_3 , days				
1997 XF11	03.10.2029	170.808	76.067	148.633	3.185	4.799	10.196	25.216
2005 YU55	30.08.2029	184.778	96.003	128.697	4.256	4.585	11.062	16.036
2007 JY2	10.09.2029	180.439	80.708	143.992	3.933	4.707	10.858	9.134
2013 ED28	21.10.2029	89.751	99.955	124.745	4.212	8.554	29.02	16.59
2007 RU9	06.05.2031	161.333	32.701	191.999	2.952	5.024	11.839	24.635
2009 XT6	24.05.2031	171.533	193.218	31.482	2.993	4.659	20.9	16.42

Table 3 presents the parameter \tilde{H}_{π} , the flyby altitude of the SC above a sphere with a radius equal to the planet's mean radius: $\tilde{H}_{\pi} = (r_{\pi} - R_{\text{pl}})$ in thousands of km, where r_{π} is the periapsis radius of the SC's orbit, and R_{pl} is the mean radius of the planet. The value is expressed in thousands of kilometers; $v_{\infty}, j = 0, 1, 2$ are asymptotic velocities at launch from Earth, Venus flyby, and asteroid flybys.

From Table 3, one can see that the lowest Δv_0 values in the transfer scheme in which the V-A-V segment is traversed on a 1:1 resonant orbit are achieved when the E-V transfer takes place along the second family trajectory, except for the 2013 ED28 asteroid. For this asteroid, the best transfer is with an E-V segment corresponding to a first-family trajectory.

2.2.4. Initial Conditions and Candidate Selection

Initial conditions for designing multi-asteroid trajectories are derived from the single-asteroid flyby cases presented in Table 3. Table 4 summarizes the post-flyby parameters following the second Venus gravity assist, which serve as input conditions for Algorithm 1.

Table 4: Candidate asteroids and initial data for calculating trajectories after the second Venus gravity assist

Name	$v_{\infty,3}$, km/s	$\gamma(t_3)^-, \text{deg}$	Φ, deg	t_3, UTC
1997 XF11	4.801	155.420	93.919	03.11.2030 6:20
2005 YU55	4.586	-171.821	93.743	14.10.2030 0:55
2007 JY2	4.702	125.677	93.842	20.10.2030 10:15
2013 ED28	8.556	-63.562	96.969	31.08.2030 13:52
2007 RU9	5.023	8.127	94.1	26.05.2032 16:41
2009 XT6	4.655	45.157	93.8	24.06.2032 4:30

These data serve as initial conditions for the selection procedure 1. These data includes asteroids international designation, as well as the flyby date and the initial asymptotic velocity at Venus. The candidate asteroids for subsequent arcs after the last approach to Venus are listed in Table 5

Table 5: Pairs of candidate asteroids for subsequent flybys

N	Asteroid-1	Asteroid-2	Date t_4 UTC	$\gamma(t_3)^+, \text{deg}$	$\Delta r_{\min}, \text{km}$
1	1997 XF11 (454101)	2013 BP73	26.02.2031 19:38	179.536	2494128.4
2	1997 XF11 (405212)	2003 QC10	29.01.2031 1:10	217.045	3954815.1
3	2005 YU55	1998 KM3	19.12.2030 8:23	129.219	1945531.6
4	2005 YU55	2013 BP73	25.02.2031 13:56	179.304	4572853.2
5	2007 JY2 (279744)	1998 KM3	17.12.2030 8:05	115.199	588853
6	2007 JY2	2013 BP73	25.02.2031 22:40	179.518	2646238
7	2013 ED28 (508967)	2004 VC17	13.10.2030 15:04	68.757	2454350.3
8	2007 RU9 (152685)	1998 MZ	21.09.2032 13:00	48.974	362259.98
9	2007 RU9	2013 JL22	07.09.2032 0:14	77.265	1586178.3
10	2009 XT6	1998 MZ	26.09.2032 22:40	70.168	2300541.3

2.2.5. Trajectory Optimization and Refinement

Trajectories combining flybys of several asteroids from Table 5 were refined using the method from Section 1.1. Table 6 presents the refined parameters for the trajectories of flybys of candidate asteroids in Table 5.

The candidate pairs from Table 5 were refined using the optimization method from Section 1.1. Table 6 presents the optimized parameters, where the asterisk (*) denotes values obtained after optimization.

Note that the symbol * in Table 6 indicates refined parameters determined within the method from section 1.1 .

As shown in the table above, the total Δv , calculated as the sum over all transfer segments except Δv_0 , in the best cases does not exceed 1 m/s, and only in two cases amounts to 95 m/s and 136 m/s for the flyby of asteroids 2005 YU55 and 2009 XT6, respectively. Moreover, in both of the latter cases, the largest Δv increase occurs during the final Venus flyby. The algorithm identified 10 candidate asteroids; feasible trajectories were found for 7 of them—5 of which were nearly impulse-free.

Table 6: Refined parameters of asteroid flybys obtained using the method from section 1.1 based on data from Table 5

Asteroid-1	Asteroid-2	t_4 , UTC	t_4^* , UTC	$\gamma(t_3)^+$, deg	$\gamma(t_3)^{*+}$, deg
1997 XF11	2013 BP73	26.02.2031 19:38	26.02.2031 09:28	179.536	179.719
2005 YU55	1998 KM3	19.12.2030 8:23	18.12.2030 23:51	129.219	123.066
2007 JY2	1998 KM3	17.12.2030 8:05	17.12.2030 11:43	115.199	117.352
2013 ED28	2004 VC17	13.10.2030 15:04	12.10.2030 02:47	68.757	66.296
2007 RU9	1998 MZ	21.09.2032 13:00	21.09.2032 17:28	48.974	47.994
2007 RU9	2013 JL22	07.09.2032 0:14	07.09.2032 18:16	77.265	73.320
2009 XT6	1998 MZ	26.09.2032 22:40	26.09.2032 02:57	70.168	79.185

2.2.6. Extended Multi-Asteroid Mission Sequences

Let us provide an example of a search for flight trajectories involving flybys of up to 8 asteroids. For this, the baseline for designing asteroid flyby sequences was only asteroids from the selected set when the number of flybys was less than 3. After the asteroid flybys exceeded 3, the entire set of PHAs, consisting of 2,030 asteroids, was used. The search results are presented in Fig. 10.

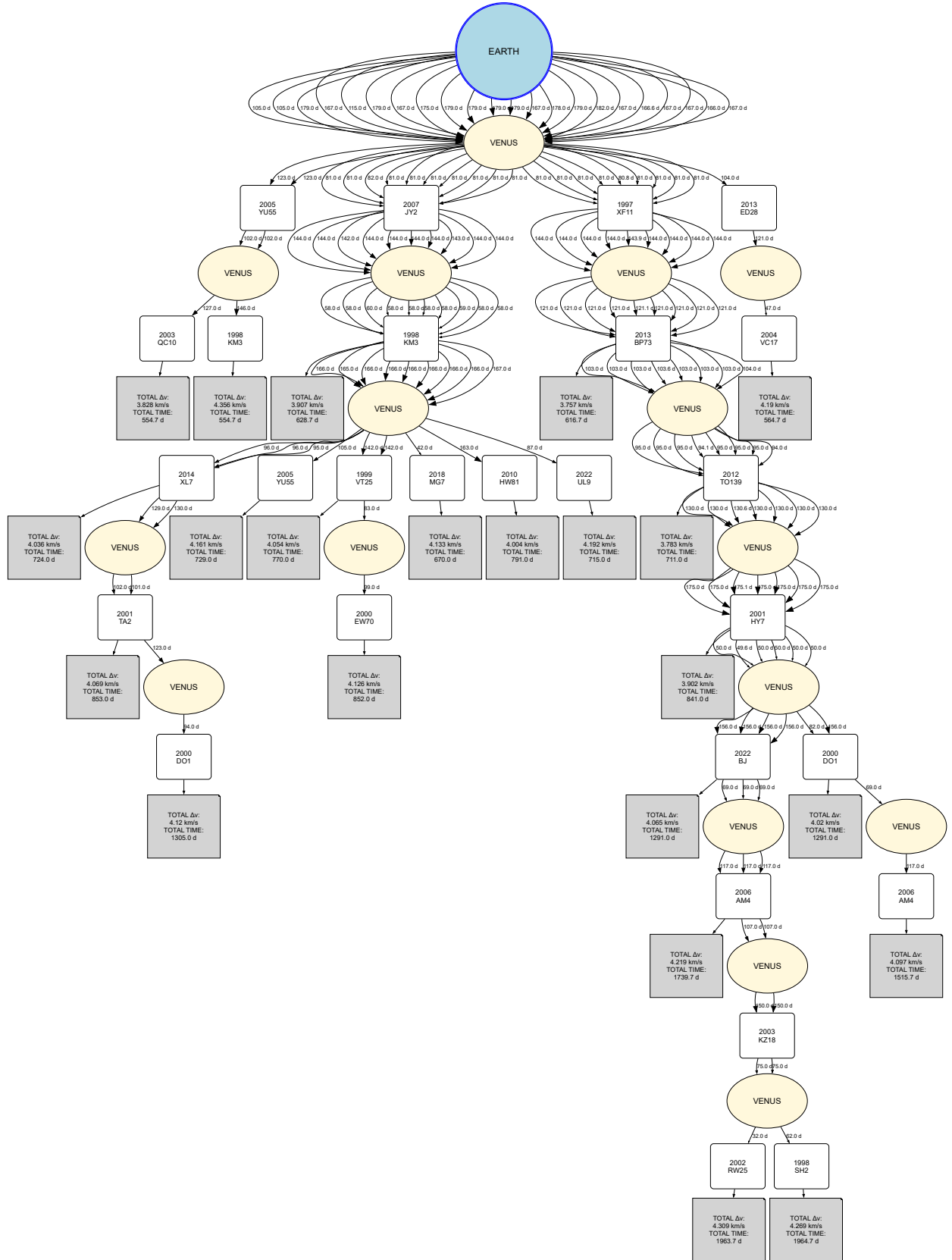


Figure 10: The tree of opportunities for asteroid flybys on a 1:1 resonant orbit includes up to eight asteroids per flight. Note that all flights end with a Venus encounter. For simplicity, the last Venus node has not been shown in this scheme.

Building upon the four single-asteroid flyby scenarios identified for the 2029 launch window, paired asteroid combinations to construct multi-target sequences were systematically enumerated. This approach revealed numerous viable scenarios with two or more asteroid encounters within the original 139-object dataset. By further extending our search to the complete PHA catalog of 2,030 objects (as of June 2025), trajectories accommodating up to eight asteroid flybys were found. The expanded catalog inclusion was necessary to access asteroids with MOID values exceeding our initial 1.05 LD threshold, thereby increasing the pool of potential targets for extended

mission sequences.

As a representative example, the construction of a spacecraft trajectory with five asteroid flybys (see Figure 10) was provided, which represents the maximum number of consecutive encounters achievable for the 2029 launch while maintaining minimal expansion beyond the initial 139-asteroid set. The five-asteroid transfer trajectory is illustrated in Fig. 11, with its principal characteristics summarized in Table 7.

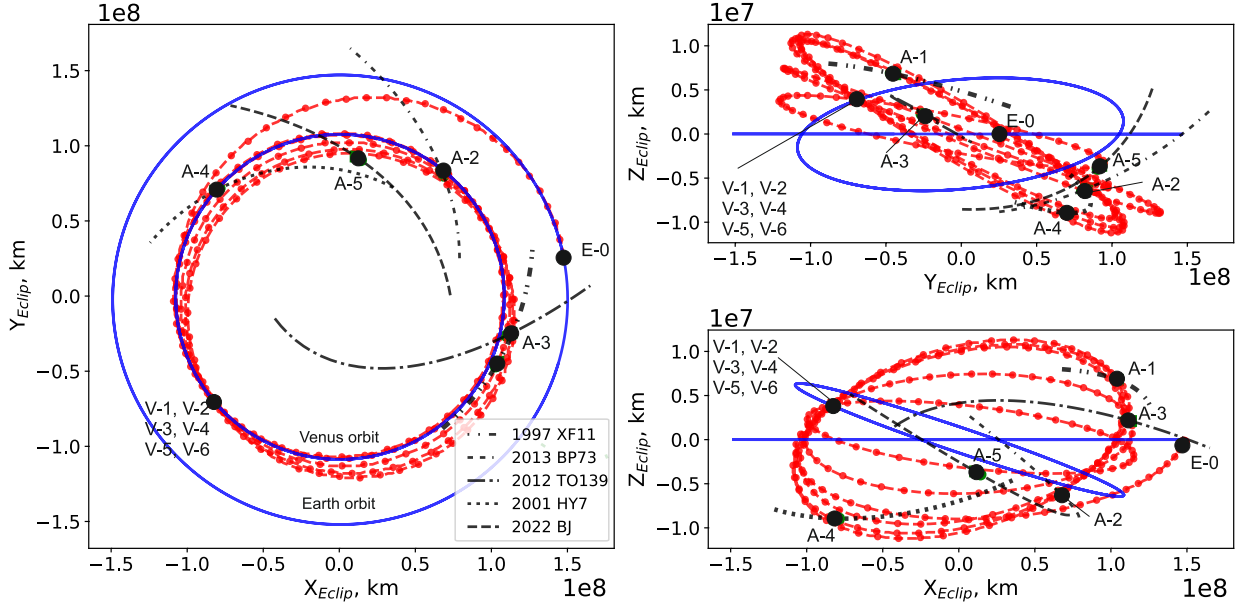


Figure 11: The trajectory of the SC of five Venus flybys and asteroid flybys on a 1:1 resonant orbit.

Table 7: Characteristics of transfer trajectories with flyby of five asteroids

Segment	Celestial Body	Path	Launch/Maneuver Date	Duration (days)	Δv (km/s)	Flyby Alt. \bar{H}_π (km)	Comm. Angle (E-SC-S, deg)	Flyby v_∞ (km/s)
Launch	Earth	Earth (E-0)	01.10.2029	-	3.757	0.2	≤ 1	3.462
1	Venus	E-0 \rightarrow V-1	17.03.2030	166.710	0.005	26607	42.68	5.070
2	1997 XF11	V-1 \rightarrow A-1	06.06.2030	80.829	0.000	-	82.71	10.081
3	Venus	A-1 \rightarrow V-2	28.10.2030	143.871	0.003	46095	174.79	5.070
4	2013 BP73	V-2 \rightarrow A-2	26.02.2031	121.098	0.000	-	105.26	21.987
5	Venus	A-2 \rightarrow V-3	09.06.2031	103.602	0.026	13136	39.30	5.030
6	2012 TO139	V-3 \rightarrow A-3	12.09.2031	94.060	0.001	-	1.38	37.189
7	Venus	A-3 \rightarrow V-4	20.01.2032	130.640	0.111	10672	99.52	4.853
8	(216523) 2001 HY7	V-4 \rightarrow A-4	13.07.2032	175.147	0.000	-	150.45	14.121
9	Venus	A-4 \rightarrow V-5	01.09.2032	49.553	0.125	3324	119.77	5.097
10	2022 BJ	V-5 \rightarrow A-5	04.02.2033	156.517	0.000	-	50.49	26.658
11	Venus	A-5 \rightarrow V-6	13.04.2033	68.183	-	-	15.39	5.096
Total				1290.210 (~3.5 yrs)	4.028			

Note that in Table 7, the angle E-SC-S denotes the Earth-SC-Sun communication angle at the moments of encounter with celestial bodies.

The data in Table 7 indicate that maneuvers V-3 and V-4 reduce the SC's orbital energy relative to Venus, while maneuver V-5 increases it, providing the necessary correction to the heliocentric orbit radius. The total Δv for these maneuvers is 270 m/s, or 0.08 ΔV_{lim}^0 . Furthermore, the magnitudes of the asteroid flyby maneuvers (A-1 through A-5) are relatively small, with a total magnitude of less than 5 m/s. Analysis of the time of flight between successive Venus flybys confirms that the SC's motion occurs along 1:1 resonant orbits, validating the initial choice of the 1:1 resonance as the primary design assumption. Therefore, for this example, the optimal SC trajectory from launch (E-0) to the final Venus encounter (V-6) consists of an Earth-Venus transfer segment followed by motion along 1:1 resonant orbits between successive Venus flybys.

Table 7 indicates that the Earth-Spacecraft-Sun (E-SC-S) angle during the second Venus flyby is 174 degrees. This angle occurs during a decreasing phase, with full solar conjunction occurring 9 days prior to the Venus flyby date. Previous studies [60, 61] have established that communication degradation typically begins at solar conjunction angles of approximately 3° – 5° (177° – 175°) for S-band, 2° (178°) for X-band, and (179°) for Ka-band. The obtained value of 174 degrees therefore falls well within acceptable communication limits.

For spacecraft following 1:1 resonant orbits, the E-SC-S angle during the second Venus flyby consistently exceeds 90 degrees. This geometric constraint arises from the orbital dynamics: optimal Δv trajectories typically yield E-SC-S angles between 0° and 45° during the initial Venus encounter. Following the gravity assist, the spacecraft completes one revolution (2π radians) in approximately 224.7 days, while Earth traverses an orbital arc of $224.7/365.25 \times 2\pi \approx 3.86$ radians (221.5°). This orbital phasing ensures that the E-SC-S

angle at the second Venus encounter always exceeds 90 degrees. As shown in Table 7, subsequent flybys occur at more favorable angles, significantly lower than the second encounter, thereby ensuring continuous radio communication with Earth throughout the mission.

2.2.7. Determination of Trajectories for SC Return to Earth after Venus Gravity Assist and Asteroid Flybys

A potential variation of the E-V-A-V scheme is to return the SC to Earth after completing a series of Venus and asteroid flybys. In this scenario, the following flight scheme is considered:

Earth → Venus → 1st Asteroid → Venus → ⋯ → Venus → p -th Asteroid → Venus → Earth.

The trajectory search method and overall approach remain unchanged, but a new Venus-to-Earth transfer segment was incorporated into the optimization. This allows for the addition of the Venus-Earth segment of flight to the optimization problem established in Section 1.1.

Let us first consider scenarios involving only one asteroid flyby. For the purpose of further analysis, let us use the results obtained in Section 2.2. Subsequently, the analysis can be carried out in the following way: comparing the parameters obtained using the E-V-A-V flight scheme with those examined in this section.

In this context, it is important to highlight the overlap between schemes that allow for a flyby with or without a return to Earth. The study period remains the same, spanning from 2029 to 2031. A list of asteroids considered for flybys is provided in Table A.1.

To compare both schemes, the following parameters are estimated in this section:

$$\Delta^2 V = \Delta v_{tot}^{EVAV} - \Delta v_{tot}^{EVAVE},$$

$$\Delta^2 T = t_0^{EVAV} - t_0^{EVAVE},$$

where the parameters denoted by *EVAV* and *EVAVE* correspond to the E-V-A-V and E-V-A-V-E schemes, respectively.

The parameters $\Delta^2 V$ and $\Delta^2 T$ represent the difference in total characteristic velocity and launch date, respectively, between the E-V-A-V-E (return) scheme and the baseline E-V-A-V (no return) scheme. Also, estimation is made in terms of changes in Δv_{tot} instead of comparing each impulse given at specific points in both schemes. This is because the studied trajectories are impulse-free and one can assume that $\Delta v_{tot} \approx \Delta v_0$.

The results of the calculations are provided in Table A.3. The estimated values of $\Delta^2 V$ and $\Delta^2 T$ are shown in Fig. 12.

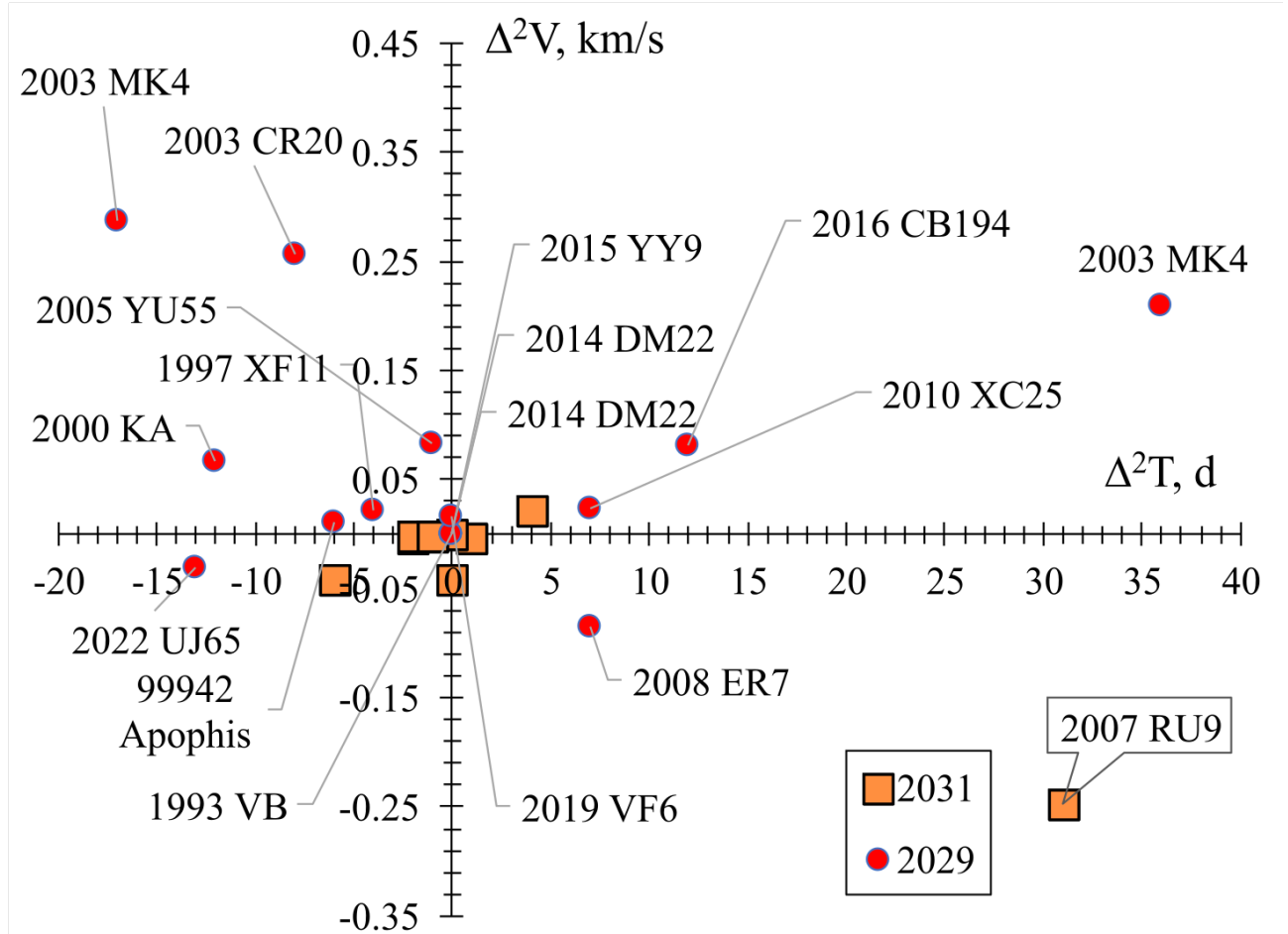


Figure 12: The change in $\Delta^2 V$ and $\Delta^2 T$ values when implementing the E-V-A-V scheme.

As a result of the study, 16 optimal return trajectories were found with launch dates in 2029 out of 35 previously obtained, and 11 out of 21 for launch in 2031. Each optimal trajectory corresponds to a unique asteroid from the selected set (see Table A.3).

The results presented in Fig. 12 show that for several trajectories with a launch in 2029, the resulting changes in Δv_{tot} are significantly smaller compared to those found in Section 2.2.1 (see Fig. 8). This reduction results from changes in the optimal duration and launch date for the Earth-Venus segment, while other trajectory characteristics remained similar to those in the previous section. Changes in the asteroid flyby velocity were also practically nonexistent, and the results fully replicate those shown in Fig. 9. The difference in duration between Venus-to-Earth transfer segments is shown in Table A.A.3, where this parameter varies from 74 to over 200 days.

For the launch in 2031, it can be seen that for 10 trajectories, the corresponding changes in $\Delta^2 V$ and $\Delta^2 T$ were negligible except for the 2007 RU9 asteroid. For the flyby of 2007 RU9 with a subsequent return to Earth after the Venus flyby, Δv_0 increased by 200 m/s while the trajectory was impulse free during the flybys of Venus and asteroids. This occurred because the optimal launch date shifted 35 days forward relative to the solution found in section 2.2.2. A similar result was observed for a scheme including a flyby of the 2003 MK4 asteroid during the launch window in 2029.

2.2.8. Detailed Example of Constructing the SC Transfer Trajectory Including Venus and Asteroid Flybys with a Subsequent Return to Earth

Let us consider an example of constructing a return trajectory to Earth after a series of Venus and asteroids flybys for the case where two asteroid flybys are included (i.e., E-V-A-V-A-V). For this, the flybys of asteroids 1997 XF11 and 2013 BP73 from Table 6 were considered. The choice of these asteroids was based on the fact that the flyby of the second asteroid occurred on a peculiar resonant orbit that has orbital parameters similar to those of Venus, but with a different inclination. Such orbits occur when $\gamma \approx 0^\circ$ or 180° , in the considered case $\gamma = 179.53^\circ$. These types of orbits have been described in references [62, 63, 64]. In this case, the SC enters Venus's SOI the second time before completing a full revolution around the Sun. In [64] such orbits are called π -resonances. Because of that, this scheme is worth constructing both in the patched-conic approach and in n -body simulations, which is shown below.

The basic parameters of flight trajectory are given in Table 8. The transfer is shown in Fig. 13.

Table 8: Characteristics of trajectory E-V-A-V-A-V-E with a subsequent return to Earth

Segment	Celestial Body	Path	Launch/ Maneuver Date	Duration (days)	Δv (km/s)	Flyby Alt. \bar{H}_π (km)	Comm. Angle (E-SC-S, deg)	Flyby v_∞ (km/s)
Launch	Earth	Earth (E-0)	01.10.2029	-	3.755	0.2	≤ 1	3.459
1	Venus	E-0 \rightarrow V-1	17.03.2030	166.948	0.005	26513	42.69	5.070
2	1997 XF11	V-1 \rightarrow A-1	06.06.2030	80.829	0.000	-	82.71	10.081
3	Venus	A-1 \rightarrow V-2	28.10.2030	143.871	0.000	46098	174.79	5.069
4	2013 BP73	V-2 \rightarrow A-2	26.02.2031	121.098	0.000	-	105.27	21.987
5	Venus	A-2 \rightarrow V-3	09.06.2031	103.602	0.001	6350	39.31	5.068
6	Earth	V-3 \rightarrow E-1	05.09.2031	88.038	-	-	42.69	7.799
Total				704.286	3.761			
							(~1.9 yrs)	

Note that the segment up to maneuver V-3 in the constructed transfer trajectory completely replicates the results given in Table 7. In particular, all maneuvers, including V-3, are found to be almost impulse free. The value of the E-SC-S angle remains high. The trajectory enables a rapid return to Earth after the final maneuver near Venus. The overall transfer duration is about two years.

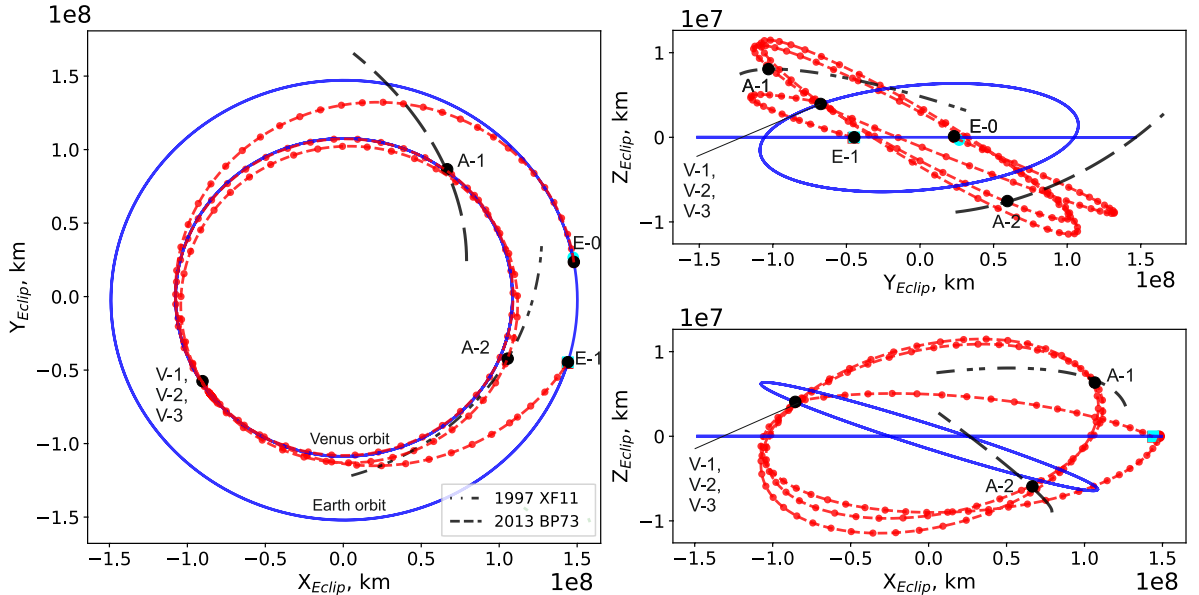


Figure 13: Trajectory of SC flyby of Venus and two asteroids on a 1:1 resonant orbit

In Fig. 13, it can be seen that the SC's flight during the asteroid flyby phase occurs in the vicinity of the Venus orbit. Note that the SC's return point to Earth differs from its initial point after the Venus and asteroid flybys tour.

2.3. Numerical Study of the Trajectory for a Flight to Venus with Asteroid Flybys and Subsequent Return to Earth

This section validates the trajectory design methodology using a high-fidelity n -body dynamical model. A concrete example featuring complete state vectors and detailed flight characteristics to demonstrate the refinement of trajectories from the two-body approximation to full n -body dynamics is presented. Two distinct optimization approaches are investigated: direct B -plane targeting and multiple shooting. The selected test case incorporates multiple asteroid flyby arcs, motion along both regular and π -resonant 1:1 orbits with Venus, and concludes with a Venus-Earth return segment, providing a comprehensive validation of the proposed mission architecture.

2.3.1. Dynamical Model of the Spacecraft Interplanetary Motion

This section presents the numerical simulation of the SC trajectory using the n -body dynamical model, focusing on the Earth-Venus-asteroid flyby sequence with subsequent return to Earth.

The equations of motion for the SC, given in a vector form, are

$$\ddot{\mathbf{r}} = -\frac{\mu}{r^2} \frac{\mathbf{r}}{r} - \sum_{j=1}^n \frac{\mu_j}{r_{j-sc}^3} \left(\mathbf{r} + \frac{3 + 3q + q^2}{1 + (1 + q)^{3/2}} q \cdot \mathbf{r}_j \right) \quad (9)$$

where \mathbf{r} is the radius vector from the central attracting body to the SC; \mathbf{r}_j is the heliocentric position vector of the j -th perturbing body; $q = \frac{\mathbf{r}}{r_j} \cdot \frac{1}{r_j} (\mathbf{r} - 2\mathbf{r}_j)$ is a function used to simplify calculations of perturbations on the right side of Eq. (9) when $\mathbf{r} - \mathbf{r}_j$ is small.

Note that this form of writing the equations using the function q is adopted based on an analysis of the study [65]. When integrating Eq. (9), the gravitational influences of the Sun, Earth, Moon, Venus, and Jupiter were incorporated. Integration was performed for the complete problem using the Dormand-Prince 7(8)-th order method on heliocentric transfer segments and the Runge-Kutta 8(9)-th order method on planet-centric segments; both methods were implemented with a modification allowing for automatic step size control.

Note that when using Eq. (9), the transition from a planet-centric segment to a heliocentric one and vice versa should occur when the following inequality is satisfied: $\frac{\mu_j}{r_{j-sc}^2} / \frac{\mu}{r^2} > 0.001$. For Earth and Venus, this ratio is reached approximately 1.4-1.7 days into the flight. In this regard, a simplification was made in this work: the transition from a planet-centric segment to a heliocentric one and vice versa occurred 2 days after or before the periapsis approach for Earth and 1.5 days for Venus.

2.3.2. Direct Approach Algorithm Based on B -plane Targeting

The transition from the two-body problem to integrating the SC trajectory using Eq. (9) was performed using the direct approach algorithm based on B -plane targeting. This plane is always orthogonal to the incoming \mathbf{v}_∞ at the planetary encounter. In this plane each approach trajectory of the SC can be described by parameters B_R, B_T . These parameters can be represented through \mathbf{v}_∞ therefore they can be used for targeting purposes [66, 67]. In this plane The core of using approach is provided in 2.

Algorithm 2: B -plane Targeting

Input: Number of segments s , minimum periapsis radius $r_{\pi,min}$
Output: Optimized trajectory parameters \mathbf{X}^* , total correction impulse Δv_{cor}
Step 1: Trajectory Segmentation;
 Divide trajectory into s segments: Earth \rightarrow Venus₁ \rightarrow Asteroid₁ $\rightarrow \dots \rightarrow$ Venus _{$s+1$} \rightarrow Earth;
Step 2: Initial Conditions and B -Plane Parameters;
for launch from Earth **do**
 | Compute $\mathbf{r}_E, \mathbf{v}_E = f_1(\mathbf{v}_\infty, 0, r_{LEO}, i_0)$;
end
foreach gravity assist maneuver $j = 1, 3, \dots, 2s - 1$ **do**
 | Compute $\mathbf{B}_j = f_2(\mathbf{v}_\infty^-, \mathbf{v}_\infty^+, r_{\pi,j})$;
end
Step 3: Boundary Value Problem;
foreach impulse time t_j **do**
 | $\Delta \mathbf{v}_j = \mathbf{v}^+(t_j) - \mathbf{v}^-(t_j)$;
 | $\mathbf{r}^-(t_j) = \mathbf{r}^+(t_j)$;
end
 $\Delta v_{cor} = \sum \|\Delta \mathbf{v}_j\|$;
Step 4: Parameter Optimization;
 Minimize $J(\mathbf{X}) = \Delta v_{cor}$ subject to $r_{\pi,j} \geq r_{\pi,min}$ using two-stage optimization method ;
return $\mathbf{X}^*, \Delta v_{cor}$

2.3.3. Example of Determining the SC Flight Trajectory by Numerical Simulation

This section presents a concrete example of trajectory determination for the E-V-A-V-A-V-E flight scheme using n -body dynamics. The initial conditions were obtained from the patched-conic approximation using the methods described in Sections 1.1 and 1.2, with specific parameters derived from the analysis in Section 2.2.

The SC state vector at LEO departure, calculated in the patched-conic approximation within the Earth's ecliptic inertial system (J2000), is given by:

$$\{\mathbf{r}_E^0, \mathbf{v}_E^0, t_{JD,UTC}^0\} = \begin{bmatrix} -5433.285187 \\ 3562.899618 \\ 981.427222 \\ -5.098547 \\ -5.328694 \\ -8.881209 \\ 2462411.308844 \end{bmatrix} \quad (10)$$

where $\{\mathbf{r}_E^0, \mathbf{v}_E^0\}$ represent the initial position and velocity vectors at periapsis, and $t_{JD,UTC}^0$ denotes the launch time from LEO. The superscript 0 indicates parameters calculated using the patched-conic approximation.

The initial time of flights on segment and periapsis radii s are given in Table 8, the B -plane components at each Venus flybys can be written as follows:

1. 1st Venus flyby $B_T = 36073.7$ km, $B_R = -24226.6$ km;
2. 2nd Venus flyby $B_T = 63359.7$ km, $B_R = -4809.2$ km;
3. 3rd Venus flyby $B_T = 4766.8$ km, $B_R = -21069.1$ km.

The SC trajectory was computed from the given initial conditions, following the sequence of asteroid encounters and planetary flybys, terminating at the return to Earth. The SC trajectory was matched by targeting specific B -plane parameters, ensuring continuity of position and velocity across planet-centric and heliocentric segments as described in Algorithm 2. During this process, impulses were applied at encounter points to maintain the feasibility of the trajectory within operational constraints. It should be noted that the boundary problems for asteroid targeting were relaxed in terms of encounter constraints. The distances from the SC to the asteroids at their closest encounter were obtained considering that the boundary problem had been solved with terminal conditions for close encounters.

The results of computation were verified using JPL's GMAT 2025 software⁸ with the Dormand-Prince 7(8)-th order method and solving boundary value problems using the classical Newton method. The DE435 ephemeris⁹ data were used to obtain the coordinates of the planets and the Moon.

The refined initial conditions of the SC at time of the transition from LEO to hyperbolic orbit, obtained after employing the trajectory optimization technique can be written as (given in the Earth ecliptic inertial system J2000):

$$\{\mathbf{r}_E, \mathbf{v}_E, t_{JD,UTC}\} = \begin{bmatrix} -5433.285186 \\ 3562.899617 \\ 981.427222 \\ -5.098547 \\ -5.328693 \\ -8.881209 \\ 2462411.778099 \end{bmatrix}$$

From comparing both (10) and (7), it can be seen that the two vectors are almost identical, with only the launch date differing by 0.46 days.

The optimized trajectory is illustrated in Fig. 14, which shows the complete E-V-A-V-A-V-E flight sequence, while Fig. 15 provides a detailed view of the SC's motion within Venus's sphere of influence.

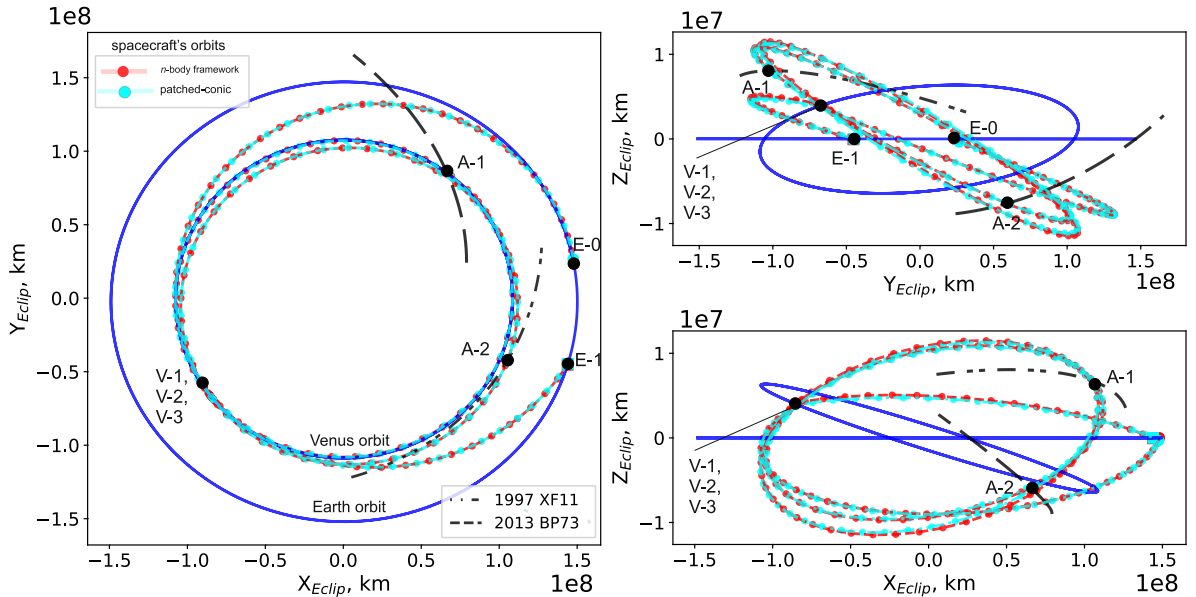


Figure 14: Complete spacecraft trajectory for Venus and dual-asteroid flyby sequence in the n -body model

The key trajectory parameters obtained from the numerical simulation are summarized in Table 9.

⁸<https://software.nasa.gov/software/GSC-19468-1> (Accessed 25.07.2025)

⁹<https://naif.jpl.nasa.gov/naif/> (Accessed 25.07.2025)

Table 9: Optimized trajectory characteristics for Earth-Venus-asteroid flyby sequence

Event	Date (UTC)	Δt (days)	B_T (km)	B_R (km)	r_π (km)	Δv (km/s)
Earth Departure	02.10.2029	–	–	–	6571	3.755*
Venus Flyby 1	17.03.2030	166.1	36130.0	-23988.7	32453.0	0.027
1997 XF11 Flyby	06.06.2030	80.9	–	–	11673.5	0.009
Venus Flyby 2	27.10.2030	143.4	60544.6	-4023.0	48850.4	0.0
2013 BP73 Flyby	26.02.2031	121.3	–	–	695035.1	0.053
Venus Flyby 3	08.06.2031	102.9	10933.3	-19180.1	12419.0	0.0

Notice that * in Table 9 denotes Δv_0 required for transition from LEO to hyperbolic orbit.

Analysis of the simulation results reveals that while the periapsis radii remain closely aligned with predictions, the B -plane parameters exhibit deviations of 165 km, 2925 km, and 6442 km in the B -vector magnitude for the three Venus flybys, respectively. These discrepancies can be attributed to two primary factors:

1. Slight temporal shifts in the Venus encounter dates and times within the n -body framework, which alter the B -plane orientation.
2. The iterative refinement process of the trajectory, where initial B -plane predictions based on \mathbf{v}_∞ are subsequently corrected during optimization.

Despite these deviations, the initial B -parameter estimates provide satisfactory first approximations for the n -body system.

Although the flyby distances vary slightly, the dates and times align precisely with the calculations, as well as the predicted periapsis radii. For example, in the case of the 1997 XF11 asteroid, the closest approach distance in the n -body simulation differs from the two-body prediction by 11673 kilometers. The closest approach for the 2013 BP73 asteroid differs by 695 thousand kilometers, which is a significant deviation from the originally intended close encounter.

The observed deviations are particularly pronounced during the second Venus flyby, where the spacecraft enters a resonant orbit approaching a π -resonance configuration (as discussed in Section 2.2.8). In this case, the spacecraft's second encounter with Venus occurs at a periapsis distance of 523,510 km, significantly deviating from the two-body prediction and complicating the design of an impulse-free trajectory for the subsequent 2013 BP73 asteroid approach.

Figure 15 illustrates the spacecraft's hyperbolic trajectories during all three Venus flybys, visually confirming the parameters presented in Table 9.

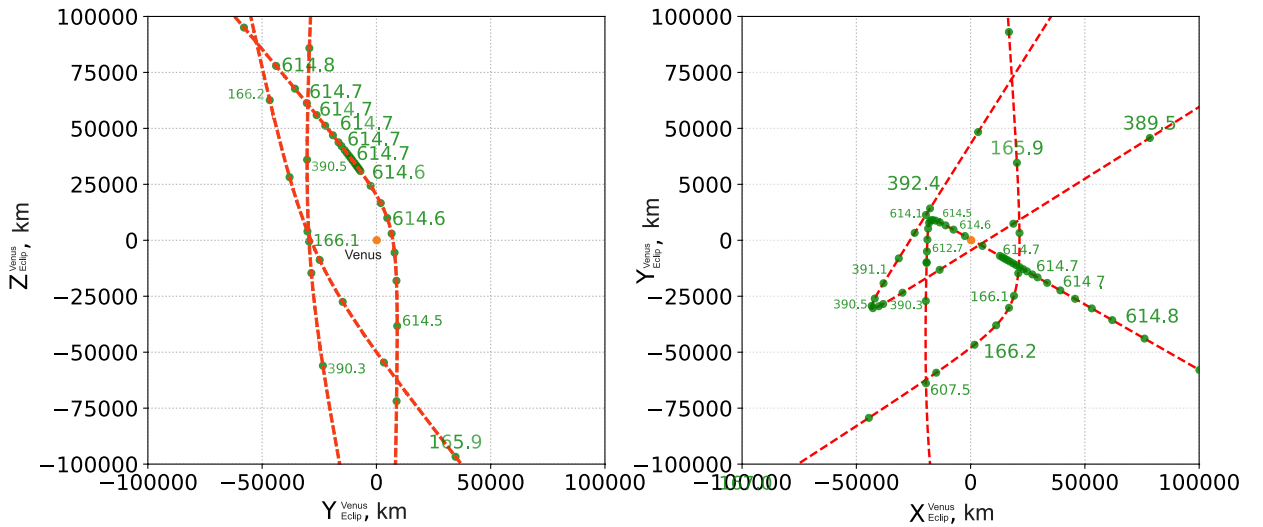


Figure 15: Hyperbolic trajectories during Venus flybys (green numbers indicate days since launch)

Let us analyze the impulses applied to correct SC trajectory at each flybys. Table 10 provides the components $[\Delta V_x, \Delta V_y, \Delta V_z]^T$ of the impulses applied during launch and at each celestial body flyby. These components represent corrections to the initial impulse values derived from the two-body dynamics analysis. To maintain consistency across all maneuvers, all impulse values are expressed in the heliocentric ecliptic coordinate system.

Notice that * in Table 10 denotes the Δv changes to the initial value, determined in the two-body approximation, Δv_0 , required for the transition from a LEO to a hyperbolic orbit.

Table 10: Maneuver ΔV Dates and XYZ Components

Maneuver	Date (UTC) (DD.MM.YYYY)	Time (UTC) (HH:MM:SS)	ΔV_x (km/s)	ΔV_y (km/s)	ΔV_z (km/s)
Earth Departure	03.10.2029	06:40:27.838	-0.0008864*	-0.0007187*	0.0033121*
1st Venus Flyby 1997 XF11	17.03.2030 06.06.2030	09:03:40.059 07:25:11.865	-0.0207574 0.0085448	0.0052086 -0.0014008	0.0300977 -0.0035252
2nd Venus Flyby 2013 BP73	28.10.2030 26.02.2031	17:15:43.555 00:20:15.191	0	0	0
Departure to Earth	08.06.2031	22:24:20.483	0	0	0

As shown in Table 10, the optimized trajectory achieves multiple asteroid encounters while maintaining Δv expenditures within the mission budget. The absence of required impulses during the second Venus flyby and Earth departure segments results from the relaxed constraints on asteroid encounter distances, as discussed in the optimization methodology.

Therefore, the results presented in this section clearly depict that the use of the direct approach algorithm based on B -plane targeting became limited to the cases when $\gamma \rightarrow 0^\circ$ or 180° . In case when solutions with such orbits appear it is necessary to use a more complex and reliable approach to refine the trajectory in an n-body model. Multiple shooting optimization techniques [68, 69] were adopted and written using the GMAT script language [70].

2.3.4. Refining Trajectory Parameters Using a Multiple Shooting Approach

The core idea of the multiple-shooting approach is to determine the spacecraft states at specific nodes $\mathbf{Y}_i \in \mathbb{R}^6$ and epochs $\mathbf{T} \in \mathbb{R}^{g+1}$, with the condition that at these nodes the spacecraft's position is continuous while its velocity changes instantaneously through an impulse maneuver $\Delta \mathbf{V}_i \in \mathbb{R}^3$.

The spacecraft states are then propagated forward and backward in time. At each point connecting the backward- and forward-propagated states, the following continuity condition is enforced:

$$\mathbf{D}_i(\mathbf{Y}_i^+, \mathbf{Y}_i^-) = \mathbf{Y}_i^+ - \mathbf{Y}_i^- = \mathbf{0}, \quad i = 0, \dots, g-1 \quad (11)$$

where the \pm superscripts denote states propagated forward (+) and backward (-) in time.

The constraints on the state vector at the initial point as well as at the terminal point can be written as:

$$\Psi_0(\mathbf{X}) = 0, \Psi_1(\mathbf{X}) = 0 \quad (12)$$

The cost function in this case can be written as:

$$\min_{\mathbf{X}} J(\mathbf{X}) = \Delta v_{cor} = \sum_{i=0}^g \|\Delta \mathbf{V}_i\| \quad (13)$$

where

$$\mathbf{X} = [\mathbf{T}, \mathbf{Y}_0, \mathbf{Y}_1, \dots, \mathbf{Y}_g, \Delta \mathbf{V}_0, \Delta \mathbf{V}_1, \dots, \Delta \mathbf{V}_g]^T \quad (14)$$

The total number of variables is: $N_x = (g+1) + 6(g+1) + 3(g+1) = 10(g+1)$.

The nonlinear constraints on the connected trajectory segments, as well as the initial and terminal points, are:

$$\mathbf{C}(\mathbf{X}) = \begin{bmatrix} \mathbf{D}_0(\mathbf{X}) \\ \mathbf{D}_1(\mathbf{X}) \\ \vdots \\ \mathbf{D}_{g-1}(\mathbf{X}) \\ \Psi_0(\mathbf{X}) \\ \Psi_1(\mathbf{X}) \end{bmatrix} = \mathbf{0} \quad (15)$$

The following algorithm was used to write a GMAT script for calculating trajectories using multiple shooting techniques.

Algorithm 3: Multiple Shooting Optimization for N Segments

Input: g (number of segments), initial guess \mathbf{X}_0
Output: Optimal trajectory \mathbf{X}^*
begin

```

     $k \leftarrow 0;$ 
     $\mathbf{X} \leftarrow \mathbf{X}_0;$ 
    while  $\|\nabla J(\mathbf{X}_k)\| > \epsilon$  and  $k < k_{max}$  do
        Unpack decision variables:  $\mathbf{T}, \mathbf{Y}, \Delta\mathbf{V} \leftarrow \mathbf{X}_k$ ;
        Apply maneuver at  $t_0$ :  $\mathbf{Y}_0^+ \leftarrow \mathbf{Y}_0 + \Delta\mathbf{V}_0$ ;
        Propagate segment forward  $(+t)$ :  $\mathbf{Y}_1^- \leftarrow \text{Integrate}(\mathbf{f}, \mathbf{Y}_0^+, t_0, t_1)$ ;
        for  $i = 2$  to  $g - 1$  do
            Apply maneuver:  $\mathbf{Y}_i^+ \leftarrow \mathbf{Y}_i + \Delta\mathbf{V}_i$ ; Propagate segment forward  $(+t)$ :  $\mathbf{Y}_{i+1}^- \leftarrow \text{Integrate}(\mathbf{f}, \mathbf{Y}_i^+, t_i, t_{i+1})$ ;
            Propagate segment backward  $(-t)$ :  $\mathbf{Y}_{i-1}^+ \leftarrow \text{Integrate}(\mathbf{f}, \mathbf{Y}_i^+, t_i, t_{i+1})$ ;
            Compute defect:  $\mathbf{D}_i \leftarrow \mathbf{Y}_{i-1}^+ - \mathbf{Y}_{i-1}^-$ ;
            Compute constraints:  $\mathbf{C}(\mathbf{X}_k) \leftarrow [\mathbf{D}_0, \dots, \mathbf{D}_{n-1}]$ ;
            Compute objective:  $J(\mathbf{X}_k) \leftarrow \sum_{i=0}^n \|\Delta\mathbf{V}_i\|$ ;
            Compute gradient:  $\nabla J(\mathbf{X}_k), \nabla \mathbf{C}(\mathbf{X}_k)$ ;
            Solve subproblem using sequential quadratic programming approach:  $\Delta\mathbf{X} \leftarrow \arg \min \frac{1}{2} \Delta\mathbf{X}^T \mathbf{H}_k \Delta\mathbf{X} + \nabla J_k^T \Delta\mathbf{X}$ ;
            Update:  $\mathbf{X}_{k+1} \leftarrow \mathbf{X}_k + \alpha_k \Delta\mathbf{X}$ ;
             $k \leftarrow k + 1$ ;
     $\mathbf{X}^* \leftarrow \mathbf{X}_k$ ;

```

For numerical integration the previously established differential equations were used 9.

2.3.5. Calculated Trajectory Parameters under Multiple Shooting Approach

Let us consider the same problem as in 2.3.3, i.e., the Earth-Venus-asteroid-Venus flight scheme. For this trajectory, the total number of variables is $N_x = 70$, with the number of nonlinear constraints equal to 34, including initial and terminal point constraints.

The refined initial conditions of the SC at time of the transition from LEO to hyperbolic orbit, obtained after employing the trajectory optimization technique from Section 2.3.4 can be written as (given in the Earth ecliptic inertial system J2000):

$$\{\mathbf{r}_E, \mathbf{v}_E, t_{JD, UTC}\} = \begin{bmatrix} -5434.309418 \\ 3562.653721 \\ 981.289719 \\ -5.127796 \\ -5.338029 \\ -8.843770 \\ 2462413.077214 \end{bmatrix}$$

The refined parameters of the trajectory, calculated using the multiple shooting approach, are given in Table 11. The required maneuvers are provided in Table 12, in the *VNB* coordinate system, where *V* is directed along the velocity vector relative to the centre body, *N* in the normal direction and *B* completes the right-handed set of vectors.

Table 11: Characteristics of the obtained SC flight trajectory

Celestial Body	Date (UTC) (DD.MM.YYYY)	Δt (days)	B_T (km)	B_R (km)	r_π (km)	Δv (km/s)
Earth	03.10.2029	165.4	-	-	6571	3.755*
Venus	17.03.2030	80.6	36130.0	-24078.2	32424.4	0.003
1997 XF11	06.06.2030	143.8	-	-	≤ 1	0.001
Venus	28.10.2030	120.9	-5120.7	63453.7	52236.3	0.117
2013 BP73	26.02.2031	103.3	-	-	≤ 1	0.010
Venus	09.06.2031	87.8	4142.9	-19985.3	11422.8	0.037

Notice that * in Table 11 denotes Δv_0 required for transition from LEO to hyperbolic orbit.

Table 12: Maneuver ΔV Dates and *VNB* Components

Maneuver	Date (UTC) (DD.MM.YYYY)	Time (UTC) (HH:MM:SS)	ΔV_V (km/s)	ΔV_N (km/s)	ΔV_B (km/s)
Earth Departure	03.10.2029	13:51:11.324	0.00001708*	-0.00003267*	0.00004652*
1st Venus Flyby	17.03.2030	22:46:01.667	-0.00048693	-0.00063599	0.00510856
1997 XF11	06.06.2030	12:20:47.452	0.00660010	-0.00486912	-0.00051071
2nd Venus Flyby	28.10.2030	06:37:18.494	0.05952555	0.06808831	0.07551561
2013 BP73	26.02.2031	03:05:04.465	0.00512191	-0.01271204	-0.00516111
Departure to Earth	09.06.2031	11:07:40.146	-0.00016309	-0.00024640	0.00432417

Notice that * in Table 12 denotes the Δv changes to the initial value, determined in the two-body approximation, Δv_0 , required for the transition from a LEO to a hyperbolic orbit.

Tables 11 and 12 show that the use of the multiple shooting method allows for a more precise restoration of the trajectory in the n -body model. The resulting Δv_{cor} is 0.15 km/s, which is about twice as high as the result obtained in the previous section, which was 0.089 km/s. While in the previous method, large discrepancies were found at flyby distances from asteroids due to relaxed constraints, in this case, the impulses compensated for these discrepancies required an additional 100 m/s impulse. It should be noted that the comparison of data from the two-body approximation and the refined data in this case differs only slightly. The total difference between the components in the B-plane does not exceed 1000 km for all three approaches to Venus.

The Table 11 and 12 analyses also show that the biggest impulse was applied at the 2013 BP73 asteroid flyby segment of the flight. This is similar to the discrepancies in asteroid flyby distances that were encountered in the previous section, as they also occur during the same flight segment.

Let us illustrate the three approaches used to calculate the trajectory discussed in Fig. 16. The figure shows the orbits of these asteroids in a rotating coordinate system, where the x-axis (X_{rot}^{Venus}) is aligned with the direction of the Sun-Venus, the z-axis (Z_{rot}^{Venus}) is directed along the orbital angular momentum, and the y-axis completes the three-dimensional basis (Y_{rot}^{Venus}). The "Venus" in upper script designates that the center of the coordinate system was placed at the center of Venus.

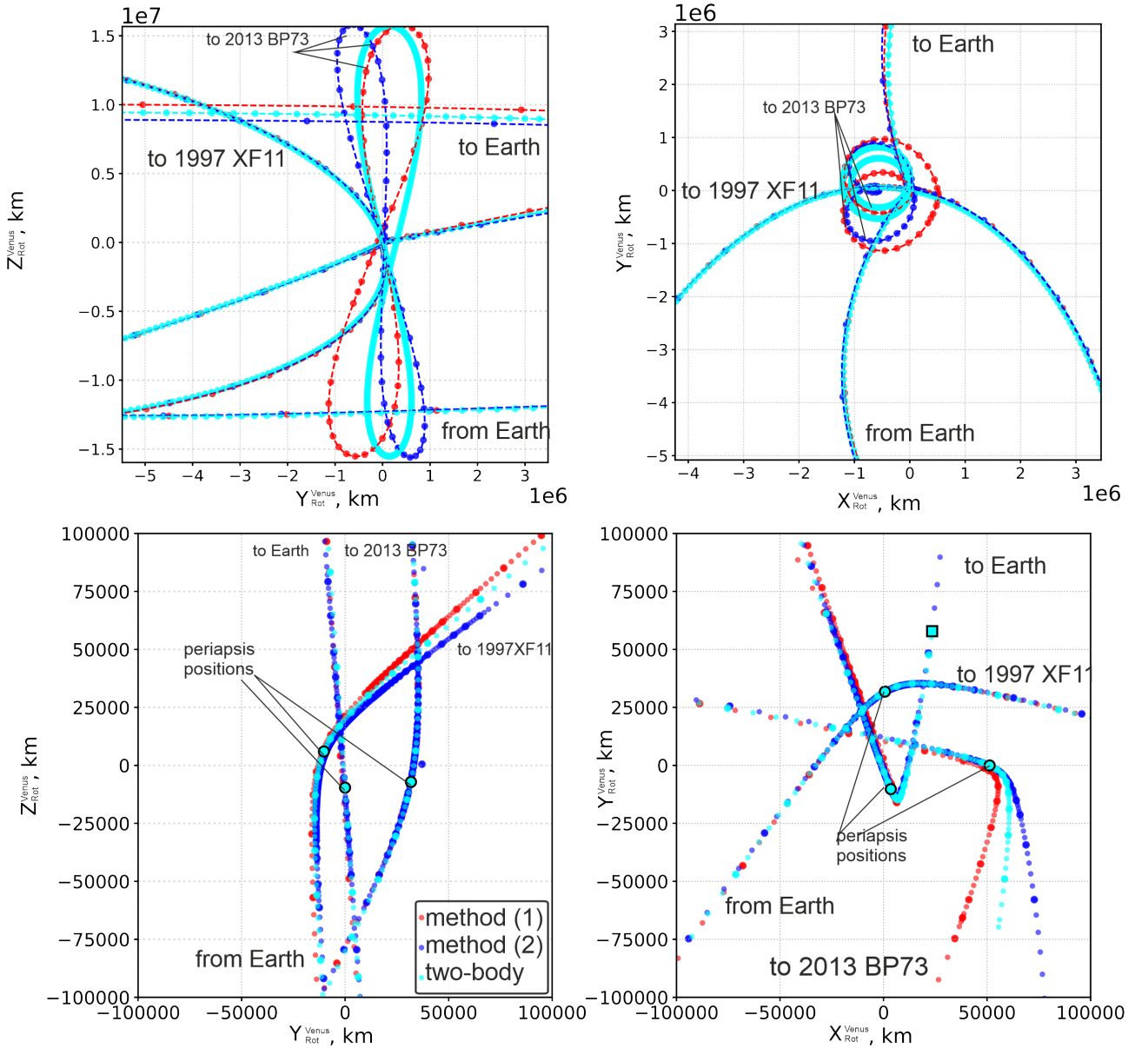


Figure 16: Hyperbolic trajectories during Venus flybys obtained using three discussed approaches in rotating coordinate system

Analysis of Figure 16 shows that the differences in trajectories calculated using the three discussed methods slightly deviate from each other starting with the first flyby and a significant deviation is indicated by impulses in the corresponding tables occurring during the flight to 2013 BP73 - entry into the π -resonant orbit.

2.4. Combining multiple Venus gravity assists with flyby of planet's resonant asteroids and PHAs

To date, approximately 20 asteroids have been identified that are in resonance with Venus orbital motion [49, 71]. These are rare objects, and their existence represents a unique phenomenon in celestial mechanics. Resonances near Venus are short-lived due to gravitational influences from giant planets and interactions with the Sun, which eventually disrupt these resonances, presenting a significant challenge to the stability of these asteroids' orbits. This study explores schemes involving flybys of potentially hazardous asteroids in conjunction with resonant asteroids.

Let us illustrate all known and suspected resonant asteroids in Fig. 17. The figure shows the orbits of these asteroids in a rotating coordinate system (X_{rot} , Y_{rot}). The remaining part of the image represents the orbits of the asteroids in the heliocentric, ecliptic J2000 frame (X_{Eclip} , Y_{Eclip}).

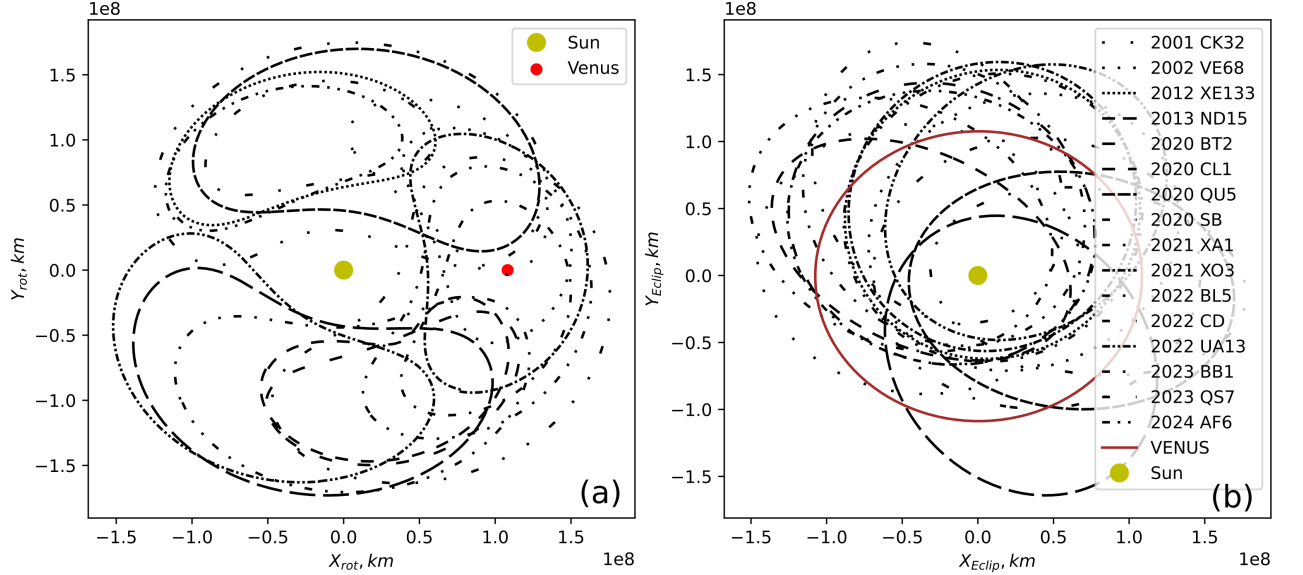


Figure 17: Resonant asteroids orbiting Venus in rotating and inertial coordinate systems for the date period 2029-2030: (a) in rotating coordinate system; (b) in the Heliocentric Ecliptic J2000 coordinate system

For the purpose of subsequent analysis, only those asteroids that make close encounters to Venus are considered. Therefore, horseshoe-type asteroids are not taken into account. Only 5 out of 20 asteroids satisfy the condition of a close encounter within 5 million km over a decade from 2029 until 2040. An example of constructing a flight trajectory using the 2001 CK32 asteroid as a target is provided. Note that the full set of PHAs was used for constructing the flight scheme.

The trajectory found is depicted in Fig. 18. Some characteristics of flight trajectory are outlined in Table 13.

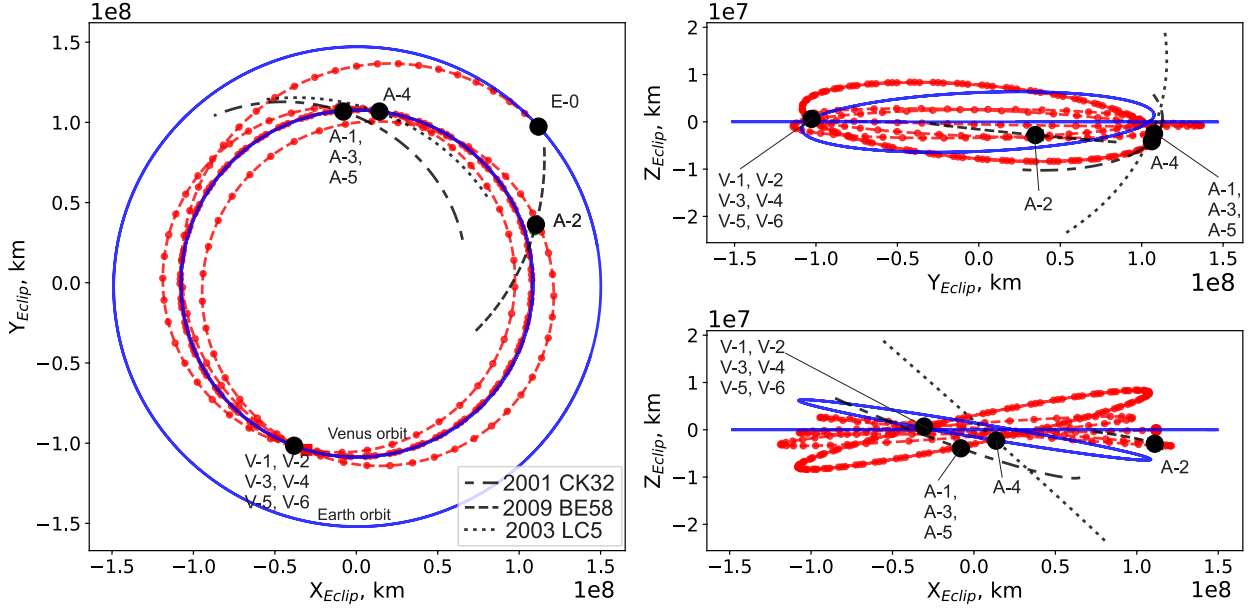


Figure 18: Trajectory of SC flyby of Venus and two asteroids on a 1:1 resonant orbit

Table 13: Characteristics of transfer trajectories with flyby of co-orbital asteroids with Venus combined with PHAs

Segment	Celestial Body	Path	Launch/ Maneuver Date	Duration (days)	Δv (km/s)	Flyby Alt. H_π (km)	Comm. Angle (E-SC-S, deg)	Flyby v_∞ (km/s)
Launch	Earth	Earth (E-0)	28.10.2029	-	3.581	0.2	≤ 1	2.823
1	Venus	E-0 → V-1	07.04.2030	160.48	0.062	6040	55.13	4.749
2	2001 CK32	V-1 → A-1	11.08.2030	126.37	0.014	-	136.63	15.281
3	Venus	A-1 → V-2	17.11.2030	98.32	0.001	1960	163.01	4.751
4	2009 BE58	V-2 → A-2	22.02.2031	96.72	0.000	-	134.29	23.274
5	Venus	A-2 → V-3	30.06.2031	127.98	0.003	2080	26.05	4.758
6	2001 CK32	V-3 → A-3	04.11.2031	126.51	0.001	-	54.13	15.332
7	Venus	A-3 → V-4	10.02.2032	98.18	0.050	14400	111.48	4.836
8	(90367) 2003 LC5	V-4 → A-4	26.05.2032	105.78	0.089	-	160.23	14.162
9	Venus	A-4 → V-5	22.09.2032	118.91	0.000	15000	106.96	4.767
10	2001 CK32	V-5 → A-5	26.01.2033	126.55	0.001	-	31.36	15.356
11	Venus	A-5 → V-6	04.05.2033	98.14	-	-	28.06	4.760
Total				1285.14	3.802			
				(~3.5 yrs)				

From Table 13, it can be seen that the trajectory found is almost impulse-free. The average flyby velocity of the 2000 CK32 asteroid is 15.3 km/s, and the flyby velocity for the planet is 4.7 km/s. The maximum value of the E-SC-S angle is 163.01 deg, which possibly allows radar observation of the SC during the first gravity assist. The next flybys of Venus occur at slightly lower angle values, and at the last planet's flybys, the E-S-C angle takes a value of 28.03 deg.

2.5. Determining Asteroid Flyby Trajectories on the Earth-Venus Transfer Segment

In the work [39], trajectories of flybys of asteroids whose orbits are in resonance with Venus were found for the Earth-Venus transfer segment. The study [40] was unable to find trajectories for flybys of asteroids larger than 1 km in diameter in the same transfer segment. This work supplements these previous studies by investigating flybys of PHAs during the Earth-Venus transfer segment.

The search largely followed the methodology outlined in Section 1.1. A significant simplification was made by considering only two transfer segments: from Earth to asteroid and from asteroid to Venus. Flybys of potentially hazardous objects from the main sample of 139 asteroids were considered. Launch periods between 2029 and 2050 were investigated.

Some parameters of calculated transfer trajectories are presented in Table 14

Table 14: Parameters of the Earth-Asteroid-Venus transfer trajectories

Name	t_0 (DD.MM.YYYY)	t_1 -/-	t_2 -/-	Δt_{E-V} (days)	Δv_0 (km/s)	$v_{\infty,0}$ (km/s)	$v_{\infty,1}$ (km/s)	$v_{\infty,2}$ (km/s)	$i_{eclip,0}$ (deg)
(367789) 2011 AG5	25.05.2029	16.12.2029	10.08.2030	442	3.695	3.246	12.007	4.817	1.896
(826936) 1998 HH49	11.12.2030	13.07.2031	05.02.2032	421	3.625	2.994	9.474	2.733	2.842
2018 BT6	03.01.2031	27.05.2031	21.03.2032	443	3.905	3.927	30.581	4.363	5.414
(177049) 2003 EE16	06.02.2031	18.06.2031	31.01.2032	359	3.947	4.05	20.003	6.868	1.183
2010 JE88	12.02.2031	07.08.2031	08.02.2032	361	3.884	3.747	31.978	7.776	0.489
(509456) 2007 LF	03.04.2031	01.06.2031	17.10.2031	197	3.793	3.579	11.177	4.41	0.781

Table 14 – continued

Name	t_0 -	t_1 (DD.MM.YYYY)	t_2 -/-	Δt_{E-V} -/-	Δv_0 (days)	$v_{\infty,0}$ (km/s)	$v_{\infty,1}$ (km/s)	$v_{\infty,2}$ (km/s)	$i_{eclip,0}$ (km/s)	$i_{eclip,0}$ (deg)
(308635) 2005 YU55	09.04.2031	13.09.2031	05.11.2031	210	4.008	4.226	15.818	5.702	1.142	
(143487) 2003 CR20	25.11.2033	05.04.2034	20.03.2035	480	4.033	4.12	16.116	3.21	1.647	
2014 SP142	24.03.2034	16.06.2034	12.06.2035	445	3.755	3.35	17.922	5.789	3.08	
(141495) 2002 EZ11	06.04.2034	01.11.2034	14.04.2035	373	4.071	4.136	22.492	8.439	2.883	
(101869) 1999 MM	08.08.2034	28.11.2034	04.02.2035	180	3.796	3.59	21.571	6.086	3.246	
(177049) 2003 EE16	22.09.2034	21.12.2034	09.03.2035	168	3.817	3.657	26.327	7.893	0.333	
2008 DJ	21.09.2035	05.12.2035	31.10.2036	406	3.903	3.922	10.481	4.488	4.273	
2021 SX3	08.01.2036	31.07.2036	09.03.2037	426	4.065	4.382	23.181	6.978	4.125	
2014 SP142	29.08.2037	04.04.2038	04.11.2038	432	3.895	3.897	8.621	8.542	1.464	
2003 MK4	06.12.2040	04.01.2041	07.05.2041	152	3.598	2.886	13.907	3.07	1.255	
2020 BC6	09.04.2042	16.09.2042	11.04.2043	367	3.863	3.802	14.487	7.579	2.669	
(85236) 1993 KH	18.09.2045	20.11.2045	30.03.2046	193	3.895	3.898	14.208	5.539	0.871	
2013 ND24	03.10.2045	14.01.2046	07.04.2046	186	3.796	3.593	29.243	5.668	0.045	
(1864) Daedalus 1971 FA	22.03.2047	13.08.2047	13.06.2048	449	4.033	4.252	20.892	8.868	0.993	
2008 MP1	24.05.2047	31.08.2047	28.11.2047	188	3.893	3.733	9.81	6.456	3.019	
2022 AY1	22.04.2048	07.07.2048	11.08.2049	476	3.909	3.813	17.052	5.417	4.307	
(89958) 2002 LY45	20.06.2048	12.01.2049	28.08.2049	434	3.577	2.609	29.81	3.84	0.664	
2014 XL7	30.06.2048	22.09.2048	20.09.2049	447	4.032	4.292	16.247	4.401	7.069	
1997 XF11	24.08.2048	16.03.2049	14.11.2049	447	3.833	3.462	18.768	6.438	3.165	

Note: t_i , $i = 0, 1, 2$, corresponds to the characteristic dates of launch, asteroid flyby and Venus encounter; Δt_{E-V} is the duration of the Earth-Venus transfer, d; $v_{\infty,i}$, $i = 0, 1$, correspond to asymptotic velocities at the times of launch and asteroid flybys. $i_{eclip,0}$ is the inclination of the SC's orbit in the Earth-to-Venus section.

As a result of the study, the findings of which are presented in Table 14, it was established that even when using the limited sample of asteroids filtered by the MOID parameter value, considered in this work, it is possible to identify several impulse-free approach trajectories for the SC with an asteroid during an Earth-Venus transfer.

However, these opportunities are significantly limited compared to those considered in Section 2.2. Only 8 out of the 25 identified trajectories for the launch period from 2029 to 2050 reached Venus in less than a single revolution. This is considerably fewer than the 56 trajectories found for the E-V-A-V scheme, which were identified for just the first two launch windows in the same period.

3. Discussion

The problem of multiple asteroid flybys has been previously studied. As stated in the introduction, many algorithms have been developed to address this issue. These algorithms include robust optimization techniques that are appropriate for the largest Global Trajectory Optimization Competition (GTOC). The need to create an asteroid tour with many nodes requires a large number of candidates to choose from. This explains the main focus of researchers on Main Belt asteroids and, from time to time, on NEAs [16, 17, 18, 19, 20, 21].

Consequently, significant research interest exists for designing multi-asteroid encounter trajectories in the Main Belt region. As a result, the space between Earth and Venus has remained underutilized and received less attention. The primary reasons for the limited exploration of asteroid flyby chains near Venus's orbit are the significantly smaller asteroid population compared to the Main Belt and the proximity to the Sun, which requires additional solutions to manage the thermal load on the SC during prolonged periods.

Growing interest in in-situ studies of Mercury and Venus, coupled with advances in small satellite technology presents opportunities to enhance the scientific return from inner Solar System missions.

To address this, the present work investigates schemes for designing SC trajectories that enable the simultaneous study of a planet and an asteroid through repeated flybys of both celestial bodies. The proposed approach uses Venus gravity assists to transition the spacecraft into resonant orbits, enabling subsequent asteroid flybys.

Particular attention was paid to the 1:1 resonance scenario, which minimizes the time intervals between flybys. Potentially hazardous asteroids ($\rho_{MOID} \leq 1.05LD$) were chosen as objects of study by SC. A comparative analysis of two strategies was conducted within four flight schemes:

- flight through the inner Solar System with a Venus gravity assist and movement along a resonant orbit;
- direct flight from Earth to an asteroid with a subsequent return to Earth.

The results obtained using the proposed approach show that the flight scheme involving Venus flybys and asteroid encounters:

- did not significantly increase the total mission duration (from launch to the first encounter with the planet after the asteroid flyby);
- in some cases, allowed for a reduction in the required characteristic velocity for the asteroid flyby;
- expanded launch opportunities by providing shorter intervals between launch windows, while maintaining the necessary characteristic velocity for the flight to the asteroid;

- in several cases, the analysis revealed that the asymptotic velocity of an asteroid's flyby was lower than that for a direct flight.

The n -body simulation of a spacecraft trajectory, including flybys of 1997 XF11 and 2013 BP73 asteroids, demonstrated the feasibility of the developed method. This confirms the ability to construct trajectories that enable asteroid flybys while the spacecraft remains near Venus's orbit. The flyby of the second asteroid highlighted a significant challenge in applying the developed trajectory search technique. It was shown that asteroid flybys on π -resonant orbits complicate refinement in n -body simulation. Although most of the predicted parameters from the patched conic method differed only slightly, the closest encounter distance for the 2013 BP73 asteroid increased to 695 thousand kilometers. This was due to the second encounter with Venus on its way to the asteroid. Because of perturbations from that encounter, it was impossible to find a close approach trajectory using this method. The latter suggests that direct refinement of trajectories using B -plane targeting is possible if the initial solution has $0^\circ \ll \gamma \ll 180^\circ$.

To handle the problem, disregarding the resonant orbit, the multiple shooting approach was used. The rationale for using it, despite its complexity, is that it uses patching between backward and forward time propagation, therefore being less sensitive to small perturbations caused by Venus and Earth in the heliocentric segment. The results of this technique showed that, in the case of strict restrictions on asteroid flyby distances, the total impulse for maneuvers increased to 0.15 km/s. The magnitude of the impulse needed for flight at $\gamma \approx 179^\circ$ is 0.11 km/s, while flight in all other segments requires less than 40 m/s in total. It can also be noted that the obtained results are close to the patched conic ones. It is known that a patched cone provides a lower limit on Δv , so the obtained result is about 5% of ΔV_0^{lim} , which means trajectories are feasible.

The importance of accounting for orbital uncertainties and their impact on flyby feasibility is acknowledged, with a comprehensive investigation of these aspects being planned for subsequent dedicated research. The development of techniques to validate trajectory solutions within high-fidelity n -body simulations that explicitly incorporate asteroid orbital uncertainties is intended for future work. Various methods, including Monte Carlo simulations and approaches based on min-max principles, will be explored to assess solution stability and resulting variations in Δv_0 requirements.

For the current study, a full uncertainty analysis was considered beyond the primary scope of establishing the fundamental feasibility of the proposed flight schemes. However, to partially address these concerns, an additional filter was incorporated into the asteroid selection process. Only asteroids with orbital element uncertainties below specific thresholds, as reported in the JPL and Minor Planet Center databases, were considered, ensuring that the candidate set was comprised of objects with well-determined orbits. Diagrams illustrating the distribution of these orbital errors for the selected asteroids have been included in Section 2.1, providing transparency regarding the quality of data utilized in the analysis.

The analysis presented was also extended from studying flybys of PHAs to co-orbital asteroids with Venus, a small population of objects that are in short-term resonance with the orbit of Venus. Trajectory construction, including a flyby of the 2001 CK32 asteroid, showed that such a scheme was feasible. This scheme shares similarities with the Lucy mission trajectory design [21] but shifts focus from Jupiter Trojans to Venus co-orbitals and from Main Belt asteroids to PHAs. The provided example demonstrates that it is possible to combine flybys of co-orbital asteroids with Venus and PHAs with a study of Venus, thus possibly expanding the scientific value of the mission.

4. Conclusions

This work presents a method for designing SC trajectories that enable the simultaneous study of a planet and an asteroid through repeated flybys of both celestial bodies. The proposed approach is based on the use of a Venus gravity assist to transition the SC into a resonant orbit, enabling subsequent asteroid flybys. To optimize calculations, a modified patched-conic method with a simplified procedure for searching for resonant orbits relative to Venus was used. For missions with multiple asteroids, geometric criteria for selecting trajectories based on orbital elements of the resonant orbit and asteroid were developed.

An advantage of the proposed flight schemes is their applicability to limited object sets. For instance, trajectories involving flybys of 1 to 3 objects were found within a set of 139 asteroids. Furthermore, trajectories involving flybys of more than two asteroids are easily found within an expanded set of selected asteroids. An analysis of the trajectory calculated for flybys of 1997 XF11, 2013 BP73, 2012 TO139, 2001 HY7, 2022 BJ asteroids in a launch window of 2029 revealed that the trajectories allow for impulse-free flybys, with the magnitude of the impulses required for planetary flybys being less than 100 m/s.

The possibility of returning the SC after a series of encounters with a planet and asteroids was investigated. The trajectories of the E-V-A-V scheme were taken and the analysis revealed that for about half of them it was possible to construct a return segment from Venus to Earth, although adding this segment to optimization changes the optimal launch date and increases Δv_0 while maintaining impulse-free asteroid flybys. The trajectory was calculated including the flybys of 1997 XF11, 2013 BP73 and return to Earth in both two-body and n -body dynamics frameworks.

It was revealed that flybys of asteroids on the trajectories closely aligned with 1:1 resonant orbits having $\gamma \approx 0^\circ$ or 180° lead to a significant deviation in asteroid flyby distance which was shown in 2013 BP73 case. While such deviations

occurred, the impulses as well as B -plane parameters in n -body dynamics remained closely aligned with the patched-conic solution in terms of the time of flight, Δv , for maneuver predictions and periapsis radii at Venus flybys. The refined B -plane parameters, though different from initial approximations, provide good starting points for n -body framework optimization.

To address the issue of finding a solution to the problem of encountering with asteroids while flying along π -resonant orbits, a multiple-shooting approach was investigated. The results of this method showed that under strict restrictions on the distance of asteroid flybys, the total impulse for maneuvers in the studied flight scheme, including flybys of 1997 XF11 and 2013 BP73, and return to Earth, was increased to 0.15 km/s.

The feasibility of a joint flyby of co-orbital asteroids with Venus and PHAs was also investigated to increase the scientific return. An example of the construction of a multiple flyby scheme for the 2001 CK32 asteroid shows that such a scheme requires a launch from Earth to Venus at a characteristic velocity about 3.581 km/s, with subsequent asteroid approaches done in low Δv . The total Δv spent excluding the launch is no more than 100 m/s.

The investigation into the transfer between Earth and Venus revealed that, in certain instances, impulse-free asteroid flybys are feasible. However, such scenarios are uncommon even for a predefined group of asteroids. For example, 25 feasible trajectories were identified from the set of 139 asteroids over a 20-year study period, compared to 56 options identified in two years of launches studied using the proposed schemes.

Appendix A Characteristics of the Earth-Asteroid-Earth and Earth-Venus-Asteroid-Venus flight trajectories

Tables A.1 and A.2 contain a set of parameters describing the SC's flight trajectories to asteroids using schemes E-V-A-V (Table A.1) and E-A-E (Table A.2). Table A.3 shows data on optimal flight trajectories found using the E-V-A-V-E scheme.

Tables A.1, A.2 contain some parameters characterizing the SC's flight trajectories to asteroids and subsequent return to the planet.

Table A.1: Some parameters of the Earth-Venus-Asteroid-Venus flight trajectories

Name	t_0	t_1	t_2	t_3	P_{sc} (day)	Δv_0 (km/s)	\bar{H} (km)	$v_{\infty,0}$ (km/s)	$v_{\infty,1}$ (km/s)	$v_{\infty,2}$ (km/s)	$i_{eclip,1}$ (deg)
(35396) 1997 XF11	29.11.2029	17.05.2030	12.08.2030	09.08.2031	449.4	3.881	3.959	3.859	6.82	5.026	3.723
(37638) 1993 VB	02.10.2029	12.03.2030	11.09.2030	05.06.2031	449.4	4.029	0.501	4.161	6.11	16.328	3.907
(85236) 1993 KH	29.10.2029	17.02.2030	28.10.2030	23.12.2031	337.06	3.886	18.528	3.874	4.072	16.057	3.838
(99942) Apophis 2004 MN4	30.09.2029	10.03.2030	09.02.2031	25.08.2032	449.43	4.059	4.571	4.357	6.185	10.252	2.545
(143487) 2003 CR20	01.10.2029	04.04.2030	08.05.2031	07.02.2032	337.06	3.759	2.164	3.471	5.195	14.236	1.232
(164207) Cardea 2004 GU9	27.10.2029	10.02.2030	22.10.2030	16.12.2031	337.06	3.821	2.344	3.673	4.691	12.63	4.052
(308635) 2005 YU55	17.12.2029	23.05.2030	29.12.2031	07.11.2032	449.4	4.039	4.51	4.311	7.242	2.315	3.704
(484506) 2008 ER7	06.09.2029	11.03.2030	24.04.2031	14.01.2032	337.05	3.909	42.626	3.941	4.603	26.404	2.524
(614433) 2009 KK	20.10.2029	28.04.2030	30.12.2031	13.10.2032	449.4	3.947	3.008	4.052	6.527	9.313	1.668
2003 MK4	10.10.2029	21.03.2030	28.11.2030	24.01.2032	336.93	3.732	22.317	3.306	5.155	16.616	2.857
2011 JA	11.11.2029	14.04.2030	19.07.2031	18.02.2032	337.05	3.641	26.545	3.057	5.005	22.293	3.915
2014 DM22	29.10.2029	28.04.2030	29.01.2031	21.07.2031	449.4	3.802	0.501	3.609	6.114	17.137	4.708
2016 FG60	08.11.2029	31.03.2030	22.12.2030	03.02.2032	337.06	3.748	47.55	3.431	5.568	27.328	2.308
2022 UJ65	30.10.2029	04.02.2030	12.11.2030	11.12.2031	337.05	3.837	26.791	3.722	5.409	10.958	3.578
(35396) 1997 XF11	29.11.2029	17.05.2030	12.08.2030	09.08.2031	449.4	3.881	3.955	3.859	6.813	5.027	3.723
(37638) 1993 VB	03.10.2029	12.03.2030	11.09.2030	05.06.2031	449.4	4.029	0.501	4.155	6.122	16.331	3.902
(85236) 1993 KH	30.10.2029	17.02.2030	27.10.2030	23.12.2031	337.06	3.883	18.999	3.865	4.055	16.058	3.808
(101869) 1999 MM	27.10.2029	05.04.2030	15.11.2030	08.02.2032	337.06	3.578	1.224	2.811	4.84	21.854	1.289
(141495) 2002 EZ11	23.10.2029	18.01.2030	19.02.2031	23.11.2031	337.05	4.038	17.133	4.311	8.844	41.59	2.66
(143487) 2003 CR20	28.10.2029	11.04.2030	06.05.2031	14.02.2032	337.05	3.601	5.37	2.902	5.013	14.442	1.255
(144898) 2004 VD17	19.10.2029	15.02.2030	15.10.2030	21.12.2031	337.05	3.924	27.028	3.986	4.598	23.293	3.524
(152685) 1998 MZ	27.10.2029	11.02.2030	27.03.2031	18.12.2031	337.54	3.857	0.501	3.697	4.559	10.698	3.416
(308635) 2005 YU55	06.12.2029	23.05.2030	29.12.2031	07.11.2032	449.4	3.945	4.19	4.045	7.233	2.317	3.705
(468468) 2004 KH17	25.10.2029	23.01.2030	12.04.2030	18.04.2031	449.4	3.91	3.408	3.944	7.583	20.453	4.214
(471240) 2011 BT15	27.10.2029	06.04.2030	27.05.2031	09.02.2032	337.05	3.579	42.03	2.816	4.851	14.416	1.527
(484506) 2008 ER7	13.10.2029	12.02.2030	22.04.2031	18.12.2031	337.05	3.942	5.127	4.039	4.973	26.216	4.38
(614433) 2009 KK	19.10.2029	27.04.2030	30.12.2031	12.10.2032	449.4	3.941	2.423	4.034	6.466	9.374	1.554
2016 CB194	14.11.2029	02.05.2030	06.08.2031	06.03.2032	337.05	3.754	5.781	3.454	6.022	13.248	4.124
(741081) 2005 LW3	28.10.2029	14.02.2030	04.04.2031	20.12.2031	337.06	3.854	17.614	3.774	4.281	19.705	4.374
2000 KA	19.10.2029	12.02.2030	18.10.2030	18.12.2031	337.05	3.861	26.911	3.798	4.7	7.995	3.408
2002 XO14	22.10.2029	01.04.2030	16.11.2030	08.01.2032	334.7	3.634	20.474	2.835	4.835	10.066	3.4
2010 XC25	12.12.2029	30.05.2030	02.09.2031	03.04.2032	337.22	4.008	21.787	4.184	7.648	16.918	3.353
2011 JA	04.11.2029	15.04.2030	19.07.2031	18.02.2032	337.05	3.622	26.409	2.984	5.097	22.268	3.801
2012 TO139	08.11.2029	29.03.2030	10.10.2031	13.09.2032	449.41	3.915	3.136	3.957	6.33	19.681	1.073
2013 ED28	20.10.2029	18.01.2030	28.04.2030	31.08.2030	224.7	4.003	16.59	4.212	8.554	29.02	4.822
2014 DM22	29.10.2029	28.04.2030	29.01.2031	21.07.2031	449.4	3.801	0.506	3.608	6.115	17.137	4.708
2014 SP142	16.12.2029	01.06.2030	18.08.2031	06.04.2032	337.05	4.012	10.788	4.235	7.812	15.349	5.702
2014 XL7	23.11.2029	05.05.2030	24.11.2031	19.10.2032	449.4	3.796	0.502	3.555	6.026	6.839	3.802
2015 YY9	13.11.2029	28.04.2030	03.02.2031	22.07.2031	224.7	3.717	8.061	3.328	5.744	11.469	8.094
2016 FG60	21.10.2029	25.03.2030	22.12.2030	28.01.2032	337.06	3.663	43.372	3.133	5.211	27.348	2.397
2016 XA2	20.11.2029	06.05.2030	16.08.2031	10.03.2032	337.05	3.779	27.532	3.536	6.151	24.381	2.237
2019 VF6	21.10.2029	05.02.2030	25.03.2031	11.12.2031	337.06	3.797	5.048	3.596	5.324	7.508	5.814
2022 UJ65	21.10.2029	05.02.2030	12.11.2030	11.12.2031	337.05	3.797	22.529	3.596	5.318	10.97	3.575
(85640) 1998 OX4	12.07.2031	30.12.2031	11.05.2032	24.03.2033	449.4	3.936	3.993	4.019	8.18	18.865	4.032
(137108) 1999 AN10	21.05.2031	17.10.2031	28.10.2032	03.04.2034	449.41	4.002	1.656	4.21	7.105	34.755	0.829
(141495) 2002 EZ11	29.05.2031	21.10.2031	05.03.2032	12.01.2033	449.4	3.823	4.667	3.678	6.253	25.315	0.696
(163243) 2002 FB3	23.05.2031	18.10.2031	04.01.2033	22.08.2033	337.06	4.062	24.614	4.375	7.341	16.038	5.357
(216985) 2000 QK130	24.05.2031	30.11.2031	01.11.2032	17.05.2034	449.41	3.913	1.267	3.811	6.448	15.562	3.418
(332446) 2008 AF4	10.06.2031	07.12.2031	16.07.2033	23.05.2034	449.4	3.813	1.165	3.648	6.525	16.574	5.587
(371660) 2007 CN26	07.06.2031	03.12.2031	23.11.2032	20.05.2034	449.41	3.782	0.507	3.546	6.23	17.814	5.176
(405212) 2003 QC10	31.07.2031	14.01.2032	27.06.2032	08.04.2033	449.4	4.014	3.989	4.241	9.234	19.456	2.562
(438908) 2009 XO	17.05.2031	06.11.2031	21.06.2033	10.09.2033	337.06	3.582	8.186	2.827	4.341	7.745	1.432
(523662) 2012 MU2	24.05.2031	13.11.2031	21.01.2033	17.09.2033	337.06	3.631	5.711	3.018	4.726	15.712	2.132

Table A.1 – continued

Name	t_0	t_1	t_2	t_3	P_{sc} (day)	Δv_0 (km/s)	\bar{H} (km)	$v_{\infty,0}$ (km/s)	$v_{\infty,1}$ (km/s)	$v_{\infty,2}$ (km/s)	$i_{eclip,1}$ (deg)
(530520) 2011 LT17	28.07.2031	11.01.2032	13.05.2033	14.05.2034	443.84	4.041	3.954	4.2	9.033	22.651	3.391
(614433) 2009 KK	02.06.2031	02.12.2031	07.05.2033	19.05.2034	449.41	3.807	1.858	3.626	6.284	24.285	4.955
2006 AR3	22.05.2031	05.09.2031	20.02.2033	20.02.2034	449.4	3.814	1.046	3.65	6.333	6.661	4.845
2007 JY2	04.06.2031	23.10.2031	05.06.2033	09.04.2034	449.41	3.91	3.309	3.943	6.506	25.155	0.11
2007 RU9	04.06.2031	22.09.2031	16.11.2031	03.05.2032	224.7	3.808	0.501	3.63	3.938	11.226	5.091
2009 XT6	24.05.2031	12.11.2031	23.05.2032	03.02.2033	224.7	3.624	16.37	2.993	4.656	20.903	2.986
2012 TY52	28.04.2031	03.09.2031	24.07.2032	17.02.2034	449.4	3.972	0.501	4.124	6.381	23.269	5.053
2012 UR158	01.08.2031	15.01.2032	24.02.2033	19.11.2033	337.05	4.019	17.554	4.255	9.295	21.038	2.443
2015 YY9	27.07.2031	11.01.2032	22.06.2033	28.06.2034	449.4	3.996	1.694	4.192	8.989	25.532	5.449
2016 FG60	28.05.2031	04.12.2031	09.04.2032	26.02.2033	449.4	3.908	1.893	3.925	6.702	22.899	3.913
2021 MK1	04.08.2031	18.01.2032	15.02.2033	23.11.2033	337.05	4.04	10.058	4.313	9.513	11.488	3.809
2022 CQ3	15.05.2031	14.11.2031	04.07.2032	19.09.2033	337.06	3.687	3.322	5.113	13.583	2.934	
2022 CY	20.04.2031	15.11.2031	19.08.2032	06.02.2033	224.62	4.078	0.501	4.374	6.251	18.958	7.502
(809875) 2020 BX12	26.04.2031	16.11.2031	29.08.2032	07.02.2033	449.4	3.966	1.304	4.109	6.044	22.483	4.641
2007 RU9	06.05.2031	15.10.2031	16.11.2031	26.05.2032	224.69	3.614	24.624	2.952	5.03	11.842	4.943
(85640) 1998 OX4	21.07.2031	30.12.2031	11.05.2032	24.03.2033	449.39	3.98	4.39	4.147	8.188	18.867	4.026
(216985) 2000 QK130	19.05.2031	28.11.2031	01.11.2032	15.05.2034	449.41	3.893	0.624	3.894	6.361	15.557	3.197
(438908) 2009 XO	22.05.2031	07.11.2031	06.01.2033	11.09.2033	337.05	3.585	8.891	2.838	4.301	7.718	1.491
(523662) 2012 MU2	29.05.2031	13.11.2031	21.01.2032	17.09.2033	337.06	3.636	5.832	3.036	4.692	15.721	2.143
2006 AR3	25.05.2031	05.09.2031	20.02.2033	20.02.2034	449.4	3.816	0.825	3.658	6.321	6.653	4.864
2016 FG60	30.05.2031	05.12.2031	09.04.2032	27.02.2033	449.4	3.918	2.256	3.919	6.767	22.928	3.945
2022 SF11	29.07.2031	13.01.2032	11.09.2032	06.04.2033	449.4	4.006	3.805	4.218	9.126	5.065	3.109

$t_i, i = 0, 1, 2, 3$ correspond to the characteristic dates of launch, transit of Venus and asteroid, return to Venus; P_{sc} is the period of the SC's orbit; $v_{\infty,i}, i = 0, 1, 2$ correspond to the asymptotic velocities at the time of launch, transit of Venus and the asteroid; $i_{eclip,1}$ is the inclination of the SC's orbit to the ecliptic after a Venus gravity assist. All dates are given in the UTC format (DD.MM.YYYY).

Table A.2: Some parameters of the Earth-Asteroid-Earth flight trajectories

Name	t_0	t_1	t_2	t_3	P_{sc} (day)	Δv_0 (km/s)	$v_{\infty,0}$ (km/s)	$v_{\infty,1}$ (km/s)	$i_{eclip,0}$ (deg)
(35396) 1997 XF11	11.12.2029	31.10.2031	11.12.2032	547.89	3.722	3.347	18.243	1.111	
(37638) 1993 VB	31.08.2029	12.12.2030	01.09.2031	365.24	3.547	2.68	7.782	4.587	
(90416) 2003 YK118	26.11.2029	27.12.2030	26.11.2032	547.88	3.908	3.937	17.856	3.249	
(99942) Apophis 2004 MN4	14.01.2029	13.04.2029	12.01.2030	365.28	3.225	0.013	7.36	0.005	
(101869) 1999 MM	17.12.2029	27.07.2030	17.12.2031	365.25	3.342	1.611	16.701	0.358	
(141495) 2002 EZ11	15.10.2029	01.03.2030	15.10.2030	365.24	3.468	2.325	27.218	2.95	
(152685) 1998 MZ	13.07.2029	06.12.2030	13.07.2031	365.15	3.485	2.324	15.632	0.171	
(164207) Cardea 2004 GU9	03.06.2029	22.10.2029	04.06.2030	365.25	3.32	1.453	8.184	0.36	
(177049) 2003 EE16	29.09.2029	29.10.2031	29.09.2032	547.88	3.734	3.388	11.286	0.897	
(269690) 1996 RG3	20.07.2029	29.10.2030	20.07.2031	365.25	3.345	1.63	14.48	2.951	
(279744) 1998 KM3	12.09.2029	13.10.2030	12.09.2032	547.88	3.845	3.747	11.285	2.789	
(367789) 2011 AG5	14.10.2029	09.07.2031	14.10.2032	547.85	3.848	3.753	16.663	1.614	
(373135) 2011 SD173	13.10.2029	30.04.2030	13.10.2030	365.26	3.434	2.157	10.675	0.12	
(380636) 2004 XN14	30.08.2029	25.01.2031	30.08.2031	365.45	3.629	2.875	6.725	3.176	
(415745) 2000 GV147	20.10.2029	20.05.2030	20.10.2030	365.25	3.275	1.052	11.791	1.362	
(434734) 2006 FX	07.05.2029	06.05.2031	07.05.2032	547.87	3.748	3.434	17.324	1.274	
(444193) 2005 SE71	01.01.2029	01.06.2029	01.01.2030	365.25	4.065	4.381	14.743	3.827	
(471240) 2011 BT15	09.02.2029	03.02.2031	10.02.2032	547.88	3.709	3.299	9.922	0.373	
(484506) 2008 ER7	15.02.2029	05.07.2029	16.02.2030	365.27	3.909	3.941	22.819	1.759	
(523654) 2011 SR5	08.03.2029	22.08.2029	08.03.2030	365.26	3.949	4.059	29.64	0.167	
(549948) 2011 WL2	08.06.2029	03.11.2030	09.06.2031	365.02	3.302	0.883	12.129	0.837	
2016 WJ1	10.07.2029	03.12.2030	10.07.2031	365.14	3.417	1.962	16.607	0.48	
2021 NQ5	02.08.2029	07.02.2030	02.08.2030	365.25	3.577	2.807	14.851	0.144	
(741081) 2005 LW3	10.02.2029	30.06.2029	10.02.2030	365.27	3.594	2.872	12.24	3.016	
(826936) 1998 HH49	31.01.2029	18.05.2029	31.01.2030	365.25	3.853	3.773	14.635	6.364	
2003 MK4	08.11.2029	18.06.2030	08.11.2030	365.26	3.723	3.349	12.326	1.919	
2008 DJ	01.01.2029	29.01.2030	30.12.2031	547.81	3.781	3.437	10.416	1.686	
2010 KR10	12.05.2029	26.10.2029	12.05.2030	365.27	3.513	2.533	14.652	1.77	
2013 ED28	19.07.2029	23.08.2030	19.07.2032	547.88	3.809	3.632	22.671	2.357	
2013 ND24	15.02.2029	21.01.2031	16.02.2032	547.89	3.743	3.415	25.223	1.629	
2014 SP142	16.01.2029	15.07.2029	16.01.2030	365.26	3.344	1.627	11.608	0.146	
2014 XL7	01.01.2029	29.05.2029	01.01.2030	365.25	3.289	1.192	15.749	0.548	
2018 BT6	28.10.2029	26.08.2031	28.10.2032	547.88	3.728	3.367	18.932	0.931	
2018 LK	07.08.2029	07.12.2030	07.08.2031	365.24	3.44	2.178	11.688	1.189	
2019 BC1	18.09.2029	12.02.2031	18.09.2031	365.47	3.737	3.261	17.767	4.872	
2019 LZ1	01.01.2029	31.05.2029	01.01.2030	365.25	3.972	4.124	35.6	0.679	
2020 HJ4	06.06.2029	04.11.2029	06.06.2030	365.26	3.373	1.811	14.221	1.681	
2021 TA8	26.12.2029	12.05.2031	27.12.2031	365.27	3.307	1.344	14.975	2.06	
2021 XL6	27.10.2029	23.11.2030	25.03.2031	366.21	3.227	0.183	14.016	0.004	
2022 BX1	01.01.2029	31.01.2030	01.01.2032	547.94	3.983	4.144	15.37	2.678	
2022 CQ3	14.08.2029	07.02.2030	14.08.2030	365.25	3.298	1.273	16.788	0.208	
2022 GY2	04.12.2029	04.12.2031	04.12.2032	547.88	3.814	3.648	20.734	2.687	
(35396) 1997 XF11	18.03.2031	15.05.2032	18.03.2034	547.9	3.791	3.576	19.082	2.417	
(89958) 2002 LY45	21.09.2031	24.03.2032	20.09.2032	365.26	3.238	0.541	31.949	0.165	
(90416) 2003 YK118	12.03.2031	25.03.2033	12.03.2034	547.9	3.872	3.827	9.08	3.162	
(141495) 2002 EZ11	09.11.2031	09.04.2032	08.11.2032	365.26	4.026	4.274	32.122	0.086	
(144898) 2004 VD17	25.09.2031	01.05.2032	24.09.2032	365.26	3.226	0.184	18.367	0.157	
(177049) 2003 EE16	04.03.2031	24.12.2032	03.03.2034	547.9	3.718	3.332	23.094	0.459	
(231937) 2001 FO32	03.10.2031	17.04.2032	02.10.2032	365.25	3.721	3.344	31.246	0.21	
(267337) 2001 VK5	12.05.2031	01.11.2031	12.05.2032	365.22	3.402	1.969	17.392	0.041	
(279744) 1998 KM3	05.01.2031	09.12.2032	05.01.2034	547.89	3.839	3.726	21.062	3.034	
(297300) 1998 SC15	29.09.2031	20.03.2032	29.09.2032	365.25	3.492	2.439	12.307	0.126	
(308635) 2005 YU55	26.04.2031	18.10.2031	25.04.2032	365.25	3.541	2.66	11.019	0.403	
(371660) 2007 CN26	16.11.2031	05.10.2033	15.11.2034	547.87	3.776	3.			

Table A.2 – continued

Name	t_0	t_1	t_2	P_{sc} (day)	Δv_0 (km/s)	$v_{\infty,0}$ (km/s)	$v_{\infty,1}$ (km/s)	$i_{eclip,0}$ (deg)
(509456) 2007 LF	13.01.2031	06.06.2031	14.01.2032	365.26	3.296	1.254	9.448	1.683
2019 LZ1	18.05.2031	17.12.2031	17.05.2032	365.26	3.49	2.431	17.408	0.755
2016 WJ1	20.02.2031	28.05.2032	20.02.2034	548.36	3.764	3.442	8.531	0.889
(741081) 2005 LW3	09.03.2031	01.12.2032	09.03.2034	546.87	3.898	3.797	19.585	1.592
2000 TU28	19.10.2031	28.04.2032	19.10.2032	365.26	3.409	2.02	10.612	0.016
2003 MK4	19.02.2031	06.01.2032	22.08.2032	366.86	3.279	0.243	13.036	0.402
2003 RS1	28.02.2031	02.09.2031	29.02.2032	365.25	3.323	1.478	8.872	0.457
2005 WY55	26.09.2031	20.06.2033	26.09.2034	547.88	3.801	3.607	25.803	2.375
2007 RU9	06.02.2031	14.09.2031	06.02.2032	365.25	3.658	3.119	18.847	2.99
2009 XT6	22.03.2031	27.06.2032	22.03.2034	547.9	3.784	3.552	29.988	1.055
2011 DV	21.04.2031	29.10.2032	15.05.2034	552.81	3.899	3.632	6.975	0.006
2012 TO139	14.02.2031	23.09.2031	14.02.2032	365.25	3.227	0.244	32.763	0.057
2012 UR158	10.07.2031	23.11.2032	09.07.2033	365.26	3.647	3.079	27.35	3.153
2013 JL22	19.09.2031	07.11.2032	19.09.2034	547.89	3.752	3.448	19.658	1.522
2014 EG45	17.01.2031	17.02.2032	16.01.2034	547.88	3.934	4.016	11.693	4.13
2014 SP142	10.08.2031	23.12.2032	10.08.2033	365.25	4.02	4.258	17.007	0.729
2014 XL7	26.02.2031	23.10.2031	26.02.2032	365.26	3.699	3.265	14.455	4.259
2018 LK	26.05.2031	12.01.2032	26.05.2033	365.26	3.765	3.49	14.666	0.803
2018 LB1	26.05.2031	05.09.2032	26.05.2033	365.25	3.246	0.681	8.656	0.63
2019 LZ1	10.09.2031	20.10.2032	10.09.2034	547.89	3.789	3.57	34.359	2.233

Note: $t_i, i = 0, 1, 2$ correspond to the characteristic dates of launch, passage of the asteroid and return to Earth; P_{sc} is the period of the SC's orbit; $v_{\infty,i}, i = 0, 1$ correspond to the asymptotic velocities at the moment of launch and passage of the asteroid; $i_{eclip,0}$ is the inclination of the SC's orbit to the ecliptic. All dates are given in the UTC format (DD.MM.YYYY).

Table A.3: Parameters of the Earth-Venus-Asteroid-Venus-Earth flight paths

Name	t_0	t_1	t_2	t_3	t_4	Δv_0 (km/s)	\bar{H} (km)	$v_{\infty,0}$ (km/s)	$v_{\infty,1}$ (km/s)	$v_{\infty,2}$ (km/s)
(35396) 1997 XF11	25.11.2029	08.05.2030	14.08.2030	31.07.2031	27.04.2032	3.902	0.503	3.644	6.062	5.274
(143487) 2003 CR20	20.10.2029	21.03.2030	12.05.2031	24.01.2032	31.01.2033	3.857	2.511	3.781	6.075	14.004
2003 MK4	15.11.2029	01.04.2030	30.11.2030	04.02.2032	18.02.2033	3.942	33.723	4.033	6.272	15.626
2014 DM22	29.10.2029	28.04.2030	29.01.2031	21.07.2031	26.11.2031	3.801	0.529	3.608	6.116	17.137
2022 UJ65	17.10.2029	05.02.2030	12.11.2030	11.12.2031	20.11.2032	3.806	20.203	3.626	5.394	10.959
(99942) Apophis 2004 MN4	06.10.2029	13.03.2030	10.02.2031	06.06.2031	27.01.2032	4.017	5.131	4.25	6.264	10.209
(37638) 1993 VB	03.10.2029	13.03.2030	11.09.2030	05.06.2031	26.08.2031	4.029	0.501	4.154	6.126	16.332
(143487) 2003 CR20	20.10.2029	21.03.2030	12.05.2031	24.01.2032	29.01.2033	3.857	2.507	3.784	6.077	14.004
(484506) 2008 ER7	20.10.2029	21.03.2030	24.04.2031	24.01.2032	30.01.2033	3.857	6.406	3.785	6.071	26.96
2003 MK4	23.09.2029	08.03.2030	28.11.2030	12.01.2032	10.01.2033	4.02	7.038	4.254	5.795	17.461
2014 DM22	29.10.2029	28.04.2030	29.01.2031	21.07.2031	10.04.2032	3.801	0.512	3.608	6.115	17.137
(37638) 1993 VB	03.10.2029	13.03.2030	11.09.2030	05.06.2031	26.08.2031	4.029	0.501	4.153	6.127	16.333
(308635) 2005 YU55	05.12.2029	25.05.2030	25.12.2031	11.11.2032	31.05.2034	4.028	4.132	4.083	7.354	2.134
(484506) 2008 ER7	20.10.2029	21.03.2030	24.04.2031	24.01.2032	30.01.2033	3.857	6.406	3.784	6.071	26.96
2016 CB194	26.11.2029	12.05.2030	07.08.2031	16.03.2032	22.04.2033	3.836	9.319	3.721	6.501	12.961
2000 KA	07.10.2029	07.02.2030	17.10.2030	13.12.2031	24.11.2032	3.928	17.461	3.999	5.399	7.865
2010 XC25	19.12.2029	30.05.2030	02.09.2031	03.04.2032	02.05.2033	4.031	21.789	4.267	7.604	16.876
2014 DM22	29.10.2029	28.04.2030	29.01.2031	21.07.2031	26.11.2031	3.801	0.508	3.608	6.115	17.137
2015 YY9	13.11.2029	28.04.2030	03.02.2031	22.07.2031	06.12.2031	3.717	7.981	3.328	5.751	11.481
2019 VF6	21.10.2029	04.02.2030	25.03.2031	10.12.2031	19.11.2032	3.813	5.004	3.595	5.391	7.463
(141495) 2002 EZ11	30.05.2031	21.10.2031	06.03.2032	12.01.2033	03.04.2033	3.824	4.8	3.681	6.232	25.326
(163243) 2002 FB3	25.05.2031	19.10.2031	04.01.2033	23.08.2033	27.07.2034	4.065	23.372	4.379	7.343	16.077
(216985) 2000 QK130	20.05.2031	29.11.2031	01.11.2032	20.02.2032	05.05.2033	3.892	0.782	3.892	6.381	15.558
(371660) 2007 CN26	08.06.2031	03.12.2031	23.11.2032	25.02.2033	16.06.2033	3.783	0.659	3.546	6.242	17.812
(530520) 2011 LT17	27.07.2031	12.01.2032	13.05.2033	13.05.2034	23.10.2034	4.045	3.939	4.203	9.043	22.672
2007 RU9	04.05.2031	10.10.2031	22.12.2031	01.01.2033	24.08.2033	4.056	0.921	4.36	7.127	6.532
2009 XT6	30.05.2031	11.11.2031	24.05.2032	02.02.2033	09.09.2033	3.666	14.635	3.008	4.47	21.145
2012 TX52	28.04.2031	03.09.2031	24.07.2032	24.11.2032	03.05.2033	4.014	0.506	4.135	6.382	23.268
2022 CY	22.04.2031	16.11.2031	19.08.2032	07.02.2033	05.08.2033	4.08	0.501	4.339	6.263	18.97
2016 FG60	28.05.2031	04.12.2031	09.04.2032	26.02.2033	06.06.2033	3.907	1.78	3.927	6.684	22.89
(809875) 2020 BX12	27.04.2031	16.11.2031	29.08.2032	07.02.2033	22.10.2033	3.967	1.342	4.107	6.049	22.478

Note: $t_i, i = 0, 1, 2, 3$ correspond to the characteristic dates of launch, passage of Venus and asteroid, and Venus, and return to Earth; $v_{\infty,i}, i = 0, 1, 2$ correspond to the asymptotic velocities at the time of launch, transit of Venus and the asteroid; $i_{eclip,1}$ is the inclination of the SC's orbit to the ecliptic after a Venus gravity assist. All dates are given in the UTC format (DD.MM.YYYY).

5. Data availability

Full catalogs of optimal trajectories are available in the appendix.

Acknowledgments

This research was funded by the Russian Science Foundation, Grant No. 25-79-00042, <https://rscf.ru/en/project/25-79-00042/>

Declaration of competing interest

The authors have no competing interests to declare that are relevant to the content of this article.

References

- [1] J. Kawaguchi, A. Fujiwara, T. Uesugi, Hayabusa—its technology and science accomplishment summary and Hayabusa-2, *Acta Astronautica* 62 (10-11) (2008) 639–647.
- [2] Y. Tsuda, M. Yoshikawa, M. Abe, H. Minamino, S. Nakazawa, System design of the Hayabusa 2—asteroid sample return mission to 1999 JU3, *Acta Astronautica* 91 (2013) 356–362.
- [3] D. Lauretta, S. Balram-Knutson, E. Beshore, W. Boynton, C. Drouet d'Aubigny, D. DellaGiustina, H. Enos, D. Golish, C. Hergenrother, E. Howell, et al., Osiris-REx: sample return from asteroid (101955) Bennu, *Space Science Reviews* 212 (1) (2017) 925–984.
- [4] A. S. Rivkin, N. L. Chabot, A. M. Stickle, C. A. Thomas, D. C. Richardson, O. Barnouin, E. G. Farnestock, C. M. Ernst, A. F. Cheng, S. Chesley, et al., The double asteroid redirection test (dart): Planetary defense investigations and requirements, *The Planetary Science Journal* 2 (5) (2021) 173.
- [5] P. Michel, M. Küppers, A. Fitzsimmons, S. Green, M. Lazzarin, S. Ulamec, P. Abell, S. Sugita, A. Campo Bagatin, B. Carry, et al., The hera space mission in the context of small near-earth asteroid missions in the past, present and future, *Space Science Reviews* 221 (5) (2025) 1–25.
- [6] M. Pugliatti, A. Rizza, F. Piccolo, V. Franzese, C. Bottiglieri, C. Giordano, F. Ferrari, F. Topputo, The Milani mission: overview and architecture of the optical-based GNC system, in: AIAA Scitech 2022 Forum, 2022, p. 2381.
- [7] H. R. Goldberg, Ö. Karatekin, B. Ritter, A. Herique, P. Tortora, C. Prioroc, B. G. Gutierrez, P. Martino, I. Carnelli, The juventas cubesat in support of esa's Hera mission to the asteroid Didymos (2019).
- [8] R. Walker, D. Koschny, C. Bramanti, I. Carnelli, E. Team, et al., Miniaturised asteroid remote geophysical observer (m-argo): a stand-alone deep space cubesat system for low-cost science and exploration missions, in: 6th Interplanetary CubeSat Workshop, Cambridge, UK, Vol. 30, 2017.
- [9] L. McNutt, L. Johnson, P. Kahn, J. Castillo-Rogez, A. Frick, Near-earth asteroid (nea) scout, in: AIAA Space 2014 Conference and Exposition, 2014, p. 4435.
- [10] L. Johnson, J. Castillo-Rogez, J. Dervan, L. McNutt, Near earth asteroid (nea) scout, in: International Symposium on Solar Sailing (ISSS 2017), no. M17-5751, 2017.
- [11] A. J. Ball, S. Ulamec, B. Dachwald, et al., A small mission for in situ exploration of a primitive binary near-Earth asteroid, *Advances in Space Research* 43 (2) (2009) 317–324.
- [12] P. Michel, M. Delbo, Orbital and thermal evolutions of four potential targets for a sample return space mission to a primitive near-Earth asteroid, *Icarus* 209 (2) (2010) 520–534.
- [13] P. Michel, M. A. Barucci, A. F. Cheng, et al., Marcopolo-R: Near-Earth asteroid sample return mission selected for the assessment study phase of the ESA program cosmic vision, *Acta Astronautica* 93 (2014) 530–538.
- [14] G. Cataldi, S. Marcuccio, Design of 3-D trajectory sequences for multiple asteroid flyby missions, *Aerospace Systems* 5 (4) (2022) 531–544.
- [15] D. Bender, A. Friedlander, Multi-asteroid flyby trajectories using Venus-Earth gravity assists, in: AIAA Conference on the Exploration of the Outer Planets, 1975.
- [16] A. A. Sukhanov, Trajectory design for the mission 'Hannes', *Acta Astronautica* 39 (1-4) (1996) 25–34.
- [17] A. S. Rivkin, B. A. Cohen, O. S. Barnouin, et al., The multi-asteroid encounter tour with imaging and spectroscopy (mantis): Mission design and prospects for in-situ sample analysis, in: 51st Annual Lunar and Planetary Science Conference, 2020, p. 2532.
- [18] A. A. Sukhanov, About the possibility of circling a large number of asteroids in the Main Belt, in: Upravlenie dvizheniem i navigatsiya letatel'nykh apparatov. Trudy XXVII Vserossiiskogo seminara, 2024, pp. 89–102.
- [19] A. Bellome, J. P. Sánchez, J. G. Mateas, et al., Modified dynamic programming for asteroids belt exploration, *Acta Astronautica* 215 (2024) 142–155. doi:10.1016/j.actaastro.2023.12.020.
- [20] A. M. Stickle, et al., Tour of asteroids for characterization observations (TACO): A planetary defense asteroid tour concept, *Planetary Science Journal* 5 (2024) 237.
- [21] C. Olkin, M. Vincent, C. Adam, et al., Mission design and concept of operations for the lucy mission, *Space Science Reviews* 220 (4) (2024) 47.

[22] A. De Iuliis, L. Mascolo, S. De Santi, L. Casalino, et al., Asteroid rendezvous missions with departure from earth-sun 14 and 15, in: *Advances in the Astronautical Sciences Series*, Univelt, 2020.

[23] L. Mascolo, L. Casalino, Optimal escape from Sun-Earth and Earth-Moon L2 with electric propulsion, *Aerospace* 9 (4) (2022) 186.

[24] H. Chen, Capacity of Sun-driven lunar swingby sequences and their application in asteroid retrieval, *Astrodynamic* 7 (2023) 315–330.

[25] M. Pupkov, N. Eismont, O. Starinova, K. Fedyayev, Construction of transfer trajectories of the spacecraft to asteroids passing near sun-earth libration points, *Solar System Research* 59 (5) (2025) 48.

[26] A. V. Ivanyukhin, V. V. Ivashkin, V. G. Petukhov, S. W. Yoon, Designing low-energy low-thrust flight to the moon on a temporary capture trajectory, *Cosmic Research* 61 (5) (2023) 380–393.

[27] E. Canalias, G. Gomez, M. Marcote, J. J. Masdemont, Assessment of mission design including utilization of libration points and weak stability boundaries, *ESA Advanced Concept Team* (2004).

[28] S. Yamaguchi, N. Hiraiwa, M. Bando, S. Hokamoto, D. B. Henry, D. J. Scheeres, Trajectory design for awaiting comets on invariant manifolds with optimal control, *Astrodynamic* 9 (4) (2025) 565–581.

[29] J. P. Sánchez, D. Morante, P. Hermosin, D. Ranuschio, A. Estalella, D. Viera, S. Centuori, G. Jones, C. Snodgrass, A. C. Levasseur-Regourd, et al., Esa f-class comet interceptor: trajectory design to intercept a yet-to-be-discovered comet, *Acta Astronautica* 188 (2021) 265–277.

[30] M. Rebelo, J. Sánchez, Optimizing launch window opportunities for esa's comet interceptor mission using primer vector theory, *Acta Astronautica* 219 (2024) 340–352.

[31] G. H. Jones, C. Snodgrass, C. Tubiana, M. Küppers, H. Kawakita, L. M. Lara, J. Agarwal, N. André, N. Attree, U. Auster, et al., The comet interceptor mission, *Space science reviews* 220 (1) (2024) 9.

[32] N. Eismont, M. Boyarskii, A. Ledkov, R. Nazyrov, D. Dunham, B. Shustov, On the possibility of the guidance of small asteroids to dangerous celestial bodies using the gravity-assist maneuver, *Solar System Research* 47 (4) (2013) 325–333.

[33] M. Ceriotti, J. P. Sanchez, Control of asteroid retrieval trajectories to libration point orbits, *Acta Astronautica* 126 (2016) 342–353.

[34] Y. Wang, V. V. Koryanov, A. G. Toporkov, Hazardous asteroid deflection based on “space billiard” mode: Mission analysis and trajectory design, *Astrodynamic* 9 (4) (2025) 465–479.

[35] H. Urrutxua, D. J. Scheeres, C. Bombardelli, et al., Temporarily captured asteroids as a pathway to affordable asteroid retrieval missions, *Journal of Guidance, Control, and Dynamics* 38 (2015) 2132–2145.

[36] J.-P. Sánchez, R. Neves, H. Urrutxua, Trajectory design for asteroid retrieval missions: A short review, *Frontiers in Applied Mathematics and Statistics* 4 (2018) 44.

[37] L. Ionescu, C. R. McInnes, M. Ceriotti, A multiple-vehicle strategy for near-Earth asteroid capture, *Acta Astronautica* 199 (2022) 71–85.

[38] B. T. Bolin, K. S. Noll, et al., The discovery and characterization of Earth-crossing asteroid 2024 yr4, *Icarus* 400 (2023) 115562, arXiv:2503.05694v2.

[39] A. V. Simonov, E. S. Gordienko, D. B. Dobritsa, P. E. Rozin, Analiz traektorii obleta asteroidov, koorbital'nykh s Veneroi, *Vestnik NPO im. S. A. Lavochkina* (2025) 63–72.

[40] V. Zubko, Analysis of prospective flight schemes to Venus accompanied by an asteroid flyby, *Acta Astronautica* 210 (2023) 56–67.

[41] V. A. Zubko, Analysis of spacecraft flight trajectories to Venus with a flyby of asteroids, *Solar System Research* 50 (2024) 112–125.

[42] N. A. Eismont, L. V. Zasova, et al., Venera-D mission: Ballistic and navigation aspects, *Solar System Research* 53 (2019) 578–587.

[43] L. V. Zasova, D. A. Gorinov, et al., Venera-D mission: Scientific goals and instrumentation, *Solar System Research* 51 (2017) 506–520.

[44] V. A. Zubko, N. A. Eismont, et al., A method for constructing an interplanetary trajectory of a spacecraft to Venus using resonant orbits to ensure landing in the desired region, *Advances in Space Research* 72 (2023) 161–175.

[45] J. B. Garvin, S. A. Getty, et al., Venus Flagship Mission Concept: Phase II study, *Planetary Science Journal* 3 (2022) 117.

[46] S. Smrekar, M. Dyar, et al., Veritas: A discovery-class Venus surface geology and geophysics mission, *AAS/Division for Planetary Sciences Meeting Abstracts* 48 (2016) 207.

[47] T. Widemann, R. Ghail, et al., Envision: Europe’s proposed mission to Venus, *AGU Fall Meeting Abstracts* 2020 (2020) P022–02.

[48] D. B. Dobritsa, G. O. Ryabova, E. S. Gordienko, A. V. Simonov, K voprosu otsenki meteornoi opasnosti pri perelete Zemlya–Venera, *Vestnik NPO im. S. A. Lavochkina* (2025) 45–54.

[49] N. Pan, T. Gallardo, An attempt to build a dynamical catalog of present-day solar system co-orbitals, *Celestial Mechanics and Dynamical Astronomy* 137 (1) (2025) 2.

[50] A. F. B. de Almeida Prado, A comparison of the “patched-conics approach” and the restricted problem for swing-bys, *Advances in Space Research* 40 (1) (2007) 113–117.

[51] D. Izzo, Revisiting Lambert’s problem, *Celestial Mechanics and Dynamical Astronomy* 121 (1) (2015) 1–15. doi: 10.1007/s10569-014-9587-y.

[52] K. V. Price, Differential evolution, in: *Handbook of optimization: From classical to modern approach*, Springer, 2013, pp. 187–214.

[53] J. L. Morales, A numerical study of limited memory bfgs methods, *Applied Mathematics Letters* 15 (4) (2002) 481–487.

[54] A. Mazzetti, L. Merotto, G. Pinarello, Paraffin-based hybrid rocket engines applications: A review and a market perspective, *Acta Astronautica* 126 (2016) 286–297.

[55] V. A. Zubko, Possible flight trajectories to Venus with landing in a given region, *Astronomy Letters* 48 (2022) 761–775.

[56] A. Masat, M. Romano, C. Colombo, Different perspectives on the B-plane: Perturbation effects and use for resonant flyby design, *Celestial Mechanics and Dynamical Astronomy* 134 (2) (2022) 17.

[57] N. J. Strange, R. Russell, B. Buffington, Mapping the V-infinity globe, *AAS Paper* (07-277) (2007).

[58] A. Sukhanov, Double flybys of the planet in space flights, *Cosmic Research* - (-) (2025) in press.

[59] C. Bonanno, An analytical approximation for the MOID and its consequences, *Astronomy and Astrophysics* 360 (2000) 411–416.

[60] D. Morabito, R. Hastrup, Communicating with Mars during periods of solar conjunction, in: *Proceedings, IEEE Aerospace Conference*, Vol. 3, IEEE, 2002, pp. 3–3.

[61] V. K. Srivastava, J. Kumar, S. Kulshrestha, B. S. Kushvah, Mars solar conjunction prediction modeling, *Acta Astronautica* 118 (2016) 246–250.

[62] Y. F. Golubev, A. V. Grushevskii, V. V. Koryanov, et al., Synthesizing spacecraft orbits with high inclinations using Venusian gravity assists, *Doklady Physics* 64 (1) (2019) 24–26.

[63] Y. F. Golubev, A. V. Grushevskii, V. V. Koryanov, et al., Adaptive methods of the flybys constructing in the jovian system with the orbiter insertion around the Galilean moon, *Solar System Research* 54 (4) (2020) 318–328.

[64] M. S. Konstantinov, V. V. Shevchenko, Design and ballistic analysis of launching a spacecraft into a heliocentric orbit with an inclination of 30° to the plane of the solar equator, *Vestnik Moskovskogo Aviatsionnogo Instituta* 31 (2024) 144–154.

[65] V. V. Ivashkin, A. Lan, Optimization of interplanetary trajectories using gravity assists, *Doklady Akademii Nauk* 484 (2019) 2–5.

[66] D.-H. Cho, et al., Trajectory correction maneuver design using an improved B-plane targeting method, *Acta Astronautica* 72 (2012) 47–61.

- [67] D.-H. Cho, et al., B-plane targeting method for orbit maneuver using low thrust, *International Journal of Control, Automation and Systems* 15 (4) (2017) 1729–1737.
- [68] P. An, N. N. Hai, T. Hoai, Direct multiple shooting method for solving approximate shortest path problems, *Journal of Computational and Applied Mathematics* 244 (2013) 67–76.
- [69] H. Diedam, S. Sager, Global optimal control with the direct multiple shooting method, *Optimal Control Applications and Methods* 39 (2) (2018) 449–470.
- [70] S. P. Hughes, D. J. Conway, J. Parker, Using the general mission analysis tool (GMAT), in: *AAS Guidance and Control Conference*, no. GSFC-E-DAA-TN39043, 2017.
- [71] V. Carruba, R. Sfair, R. Araujo, O. Winter, D. Mourão, S. Di Ruzza, S. Aljbaae, G. Caritá, R. Domingos, A. Alves, The invisible threat-assessing the collisional hazard posed by undiscovered Venus co-orbital asteroids, *Astronomy & Astrophysics* 699 (2025) A86.